Environmental Science Nano

ROYAL SOCIETY OF CHEMISTRY

CRITICAL REVIEW

View Article Online
View Journal | View Issue

Cite this: *Environ. Sci.: Nano*, 2024, **11**, 1784

Magnetically recyclable nanophotocatalysts in photocatalysis-involving processes for organic pollutant removal from wastewater: current status and perspectives

Zexiao Zheng,†[a] Juhua He,†[b] Zuyao Zhang,[a] Ashutosh Kumar,[c] Musharib Khan,[d] Cheuk Wai Lung[a] and Irene M. C. Lo *[ae]

Photocatalysis, a promising technology for the removal of recalcitrant organic pollutants from wastewater has attracted global attention. The rational development of photocatalysts is crucial to the circular economy of photocatalytic water treatment. Furnishing highly efficient nanophotocatalysts with magnetism allows the breakthrough and practicability of the photocatalysis-involving processes inhibited by materials' poor recoverability. The strategy of embedding magnetic components in nanophotocatalysts and obtaining the magnetically recyclable nanophotocatalysts (MRNPCs) ensures the facile separation of photocatalyst materials from the treated water. The literature from 2012 to 2023 is reviewed to discuss the recent applications, mechanisms, and challenges of MRNPCs for organic pollutant removal. Various synthesis methods provide the desirable morphologies and properties of MRNPCs and therefore can be selected based on the application. In conventional photocatalysis, element doping, heterojunction construction, and hybrid material functionalization, have been applied to modify MRNPCs for better performance. Applications of MRNPCs in the photocatalysis-involving processes, including photocatalytic Fenton-like process, photocatalytic sulfate radical-based process, photocatalytic ozonation, and sono-photocatalytic process, are also overviewed. These processes have an increased production of reactive oxygen species, which ultimately improve the performance in contaminant removal. Furthermore, the perspectives and challenges of the MRNPCs are also discussed to shed light on the practicality of the technology.

Received 5th December 2023,
Accepted 6th March 2024

DOI: 10.1039/d3en00906h

rsc.li/es-nano

Environmental significance

Organic pollutants significantly deteriorate water quality, posing risks to both ecosystems and human health. Researchers have developed magnetically recyclable nanophotocatalysts (MRNPCs) to remove recalcitrant organic pollutants, which are highly efficient and can be easily separated from treated water through external magnetic fields. This work summarizes the basic information of MRNPCs and reviews their application in conventional photocatalysis and photocatalysis-assisted processes. Specifically, the current status, mechanism, pros, and cons of MRNPCs in these processes are discussed. In addition, the remaining challenges of MRNPCs and perspectives toward industrial applications are also explored for future research.

1. Introduction

Rapid urbanization and industrialization have increased the contamination of water bodies, becoming an issue of global concern.[1,2] A report from the United Nations World Water Development showed that over 2 billion individuals inhabit regions experiencing severe water scarcity, and this number is expected to increase in the coming years.[3,4] Together with the increasing water demand, more organic pollutants, including organic dyes, pesticides, insecticides, surfactants, disinfection byproducts, pharmaceuticals, personal care products, *etc.*, are released into various water bodies through different sources and pathways.[5,6] These pollutants

[a] *Department of Civil and Environmental Engineering, The Hong Kong University of Science and Technology, Hong Kong, China. E-mail: cemclo@ust.hk; Fax: +852 2358 1534; Tel: +852 2358 7157*
[b] *School of Environment and Chemical Engineering, Foshan University, Foshan 528000, China*
[c] *Department of Energy & Environment, Thapar Institute of Engineering & Technology, Patiala, 147004, Punjab, India*
[d] *Institute of Environmental Sciences and Engineering (IESE), School of Civil and Environmental Engineering (SCEE), National University of Sciences and Technology (NUST), Sector H-12, Islamabad, Pakistan*
[e] *Institute for Advanced Study, The Hong Kong University of Science and Technology, Hong Kong, China*
† These authors contributed equally to this work.

significantly deteriorate the water quality and have negative effects on human health.[7] For example, pharmaceuticals, pesticides, and surfactants are highly toxic and carcinogenic substances that can lead to endocrine disruption and antimicrobial resistance after prolonged exposure.[8,9] In 2007, the European Union regulated certain organic chemicals as priority pollutants to protect surface water bodies from pollution.[10] Thus, developing and implementing highly efficient water treatment strategies has become of paramount importance against the escalating global water crisis.

The capacity of the existing wastewater treatment processes to treat increasingly serious pollutants (*e.g.* PPCPs) is low.[1,10] With the increasing complexity of organic pollutants present in wastewater and the demand of higher flexibility of meeting rapid varying water quality demand, the existing wastewater treatment processes are unable to achieve progressively stricter effluent regulations.[11–15] Moreover, the conventional processes have intrinsic drawbacks. Biological and chemical enhanced processes are either time-consuming or chemical-intensive, both produce sludge. Adsorption is effective, but of low treatment capacity and high material cost.[16] Typically, chemical oxidation involving chlorination and ozonation for water disinfection leads to high chemical consumption and generation of toxic by-products.[16–18] Currently, advanced oxidation processes (AOPs) are considered to be proven processes to overcome the abovementioned drawbacks.[18–21]

Among various AOPs, photocatalysis is usually preferred over other processes due to the fact that it is simple, efficient, inexpensive, and environmentally friendly.[22] However, selecting a suitable photocatalyst with high reactivity towards organic pollutants is a major challenge. Nanotechnology has driven the development of photocatalysts with nanoscale properties which have advantages arising from their unique physical and chemical properties, mainly increased volume-to-surface area ratio and quantum effect.[23,24] The high specific surface area offers more reaction sites to accelerate organic pollutant degradation with a lower photocatalyst dose required compared with bulk photocatalysts with a low specific surface area.[25] Additionally, such nanomaterials exhibit strong adsorption rate, catalytic activity, and reactivity.[26] As a result, the photocatalytic degradation process can be intensified, and the processing cost can be reduced by using nanoscale photocatalysts.[27] However, their inefficient separation from the solution after use remains a problem because it results in potential secondary pollution and a loss of valuable material.[28,29]

Magnetically recyclable nanophotocatalysts (MRNPCs) have shown good potential among the existing nanophotocatalysts to solve the recovery problem. Typically, MRNPCs are composed of magnetic nanoparticles coated with photocatalysts, such as TiO_2 and ZnO.[30–32] The magnetism provided by the magnetic materials, such as α-Fe_2O_3, γ- Fe_2O_3, Fe_3O_4, and $ZnFe_2O_4$, allows an easy separation from the treated water.[3] These MRNPCs have shown good efficiencies in the degradation of organic pollutants, along with excellent reusability. Compared with conventional photocatalysts, the MRNPCs exhibit merits of facile recovery from treated water, high scalability, enhanced reactivity for the applications on photocatalysis-involving AOPs, and less material waste during application.[3,31,32] As evident from Fig. 1, the overall trend of publications in the literature on MRNPCs is found to be increasing in the last decade. To understand the development and challenges related to MRNPCs, a review of literature published between 2012 and 2023, is conducted in this study.

Through the literature review, it is found that MRNPCs composed of pristine photocatalysts and magnetic materials face challenges of unsatisfied performance because of limited light absorption ability and high charge recombination.[33,34] Various modification methods are explored to solve this problem, such as element doping, heterojunction construction, and hybrid material development have been employed during material synthesis. Furthermore, the practical potential of the MRNPCs can be enhanced by combining photocatalysis with other AOPs, such as the Fenton process,[35] sulfate radical-based AOP,[36] ozonation,[37] and ultrasound.[38] The combinations improve the efficiency of photo-generated electron use and increase the yield of reactive species, subsequently leading to higher reaction performance of photocatalysis in practical use. This synergistic effect of the photocatalysis-assisted reaction boosts the reaction efficiency and is necessary for the practical application of the technique.

To provide a comprehensive overview of MRNPCs utilized for organic pollutant degradation, approximately two hundred publications are reviewed. The developed MRNPCs have shown various properties based on the magnetic materials, modifications, and synthetic methods applied. The mechanism and recent application of MRNPCs in photocatalysis and photocatalysis-assisted processes, and their pros and cons are also discussed. Thereafter, the current challenges and potential opportunities are explored based on reported studies.

2. Basis of MRNPCs

In general, a MRNPC consists of a photocatalyst part for producing photogenerated electrons and holes for pollutant removal and a magnetic material part for easy separation. The performance of MRNPCs in organic pollutant removal is significantly affected by the employed photocatalysts and magnetic materials, synthesis process, and magnetic separation. A detailed overview of these aspects is given as follows.

2.1 Commonly applied photocatalysts in MRNPCs

The efficiency of an MRNPC in pollutant removal mainly depends on the reactivity of the photocatalyst because it is the core for generating charge carriers. In general, the semiconductors used as photocatalysts in MRNPCs should possess the following characteristics: (i) high photocatalytic

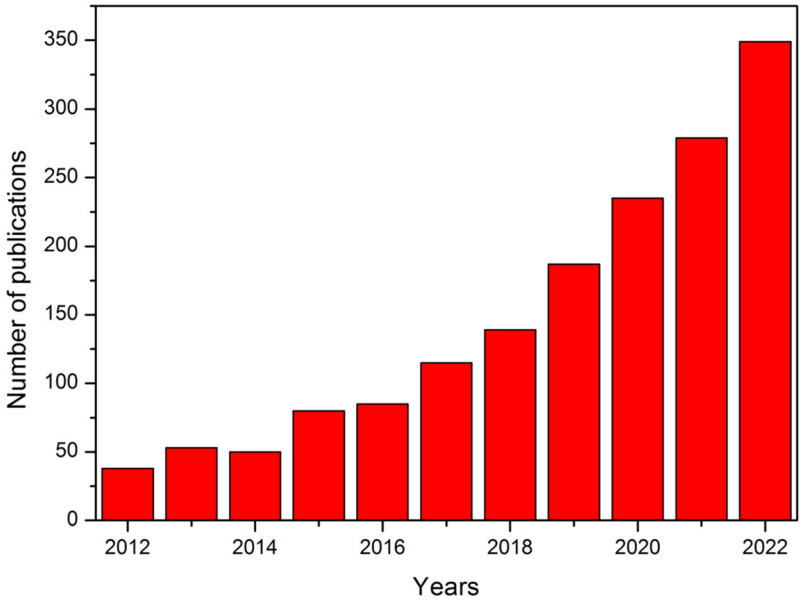

Fig. 1 The recent trends in the developments of MRNPCs between the years 2012–2022 (the raw data of this graph was obtained from the Scopus database using the keywords 'magnetic', 'nano', and 'photocatalyst').

reactivity to generate abundant charge carriers for organic pollutant degradation; (ii) good solar light absorption ability to ensure a high solar energy convention efficiency; (iii) suitable conduction and valence bands positions for initiating redox reactions; (iv) non-toxic in nature to avoid introducing additive toxicity to the treated water; and (v) good reusability and stability to ensure long-term operation and reduce secondary pollution caused by material leaching.

Fig. 2 summarizes the commonly used semiconductors as photocatalysts for MRNPC preparation, giving the band gap energies of the semiconductors and the redox energy levels of the involved reactive oxygen species in photocatalytic water treatment. Apart from TiO_2 and ZnO, the semiconductors possess band gaps narrower than 3.0 eV and are visible-light-responsive. Magnetic materials, mainly Fe_2O_3 and various spinel ferrites, can also work as photocatalysts in MRNPCs. Additionally, most of the employed semiconductors possess

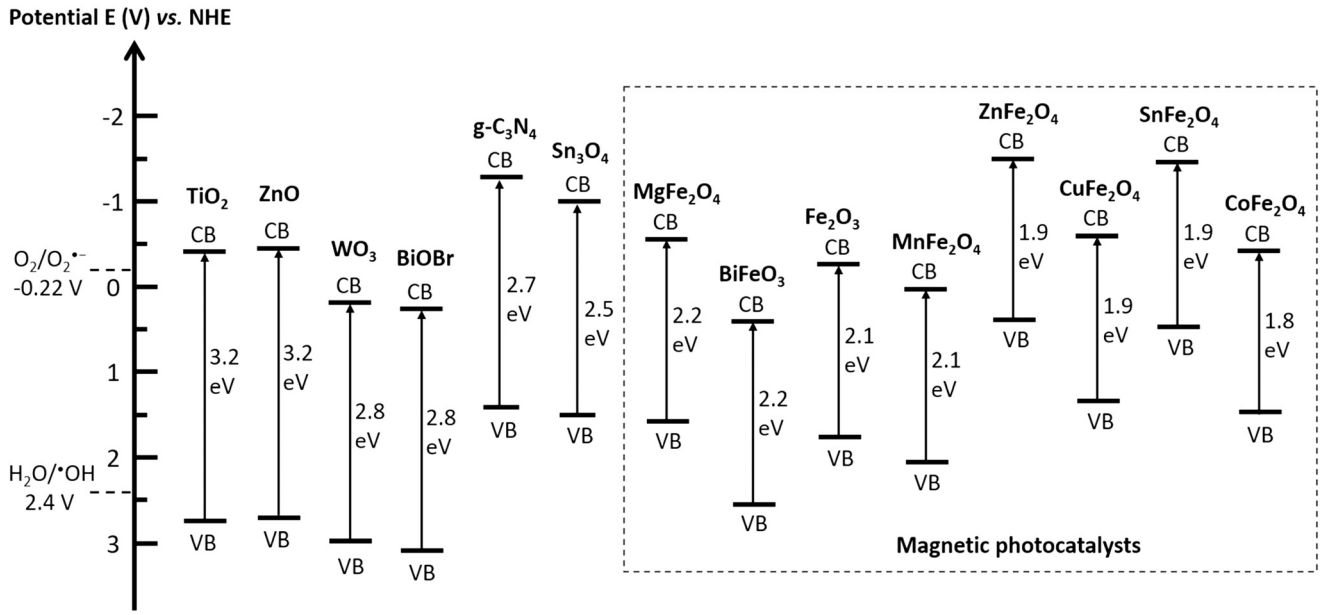

Fig. 2 Band gap energies of the involved photocatalysts in the reviewed MRNPCs and redox potentials of oxygen reduction and water oxidation to produce reactive oxygen species at pH 7.

conduction bands with more negative energy than that required for oxygen reduction or valance bands with more positive energy than that of $H_2O/^{\bullet}OH$, and therefore, afford sufficient redox energy in the production of reactive oxygen species for organic pollutant degradation.

2.2 Magnetic materials in MRNPCs

In MRNPCs, iron oxides and spinel ferrites, are usually employed to provide magnetic properties for magnetic separation. These magnetic materials possess superparamagnetic characteristics that are reversible, allowing the materials to be evenly suspended in wastewater for decontamination and ease of separation after the treatment. The properties of iron oxides and spinel ferrites in MRNPCs, their advantages, and their disadvantages are discussed in detail below.

Iron oxides, most commonly explored as Fe_2O_3 and Fe_3O_4, have a porous structure with a high surface area and are highly magnetic responsive and non-toxic.[39] Fe_2O_3 mainly exists in the crystalline forms of α-Fe_2O_3 (hematite) and γ-Fe_2O_3 (maghemite), and γ-Fe_2O_3 possesses a higher saturation paramagnetism (Ms, 60–80 emu g^{-1}) than that of α-Fe_2O_3 (0.3–11 emu g^{-1}).[40] Fe_2O_3 is a photo-response magnetic material with a narrow band gap of 2.2 eV, making it a popular choice for incorporating different semiconductors.[41–43] Notably, Fe_2O_3 is abundant in the earth and can be easily synthesized from existing resources at low cost, combining the benefits of high chemical stability and facile separation.[44] However, Fe_2O_3 is rarely used as a pristine photocatalyst for wastewater treatment due to its low photocatalytic reactivity and high charge recombination. Moreover, it also has a limited redox potential for pollutant degradation due to the unfavorable band positions. On the other hand, Fe_3O_4 has a much higher M_s (92–100 emu g^{-1}) than Fe_2O_3 but its photocatalytic activity is negligible.[44,45] Fe_3O_4 exhibits high catalytic reactivity in photocatalysis-involving AOPs, such as photocatalytic activation of hydrogen peroxide (H_2O_2), peroxydisulfate (PDS), and peroxymonosulfate (PMS), because it can provide both ferrous (Fe^{2+}) and ferric (Fe^{3+}) ions for the activation of these oxidants. Nonetheless, Fe_3O_4 is less stable than Fe_2O_3 which may suffer from photocorrosion under certain conditions.[46] Coating SiO_2 is an appropriate strategy to improve the stability of Fe_3O_4.

Spinel ferrites are a kind of bimetallic oxide with a general chemical formula MFe_2O_4, with M representing divalent metal ions, mainly Zn, Cu, Ni, Mn, Co, and Mg. Moreover, Fe^{3+} ions in MFe_2O_4 can be replaced by other trivalent ions. In general, spinel ferrites possess narrow band gaps (<2.5 eV), allowing them to utilize visible light. As a result, spinel ferrites ($MgFe_2O_4$, $CuFe_2O_4$, $ZnFe_2O_4$, $CoWO_4$, *etc.*) are widely applied as MRNPCs or a component in MRNPCs for organic pollutant removal.[45] Apart from their photocatalytic activity, spinel ferrites, especially those containing dual transition metal ions, exhibit superior catalytic activity in activating H_2O_2, PDS, and PMS because of the existence of sufficient active sites. Different from iron oxides, the cost and availability of certain metal ions in spinel ferrites, especially nickel, bismuth, and cobalt, is an important consideration.[47] Additionally, compared with iron oxides, the synthesis of spinel ferrites is much more complex, which may also increase the material cost.

2.3 Synthesis methods of MRNPCs

Several synthesis methods, including co-precipitation, thermal decomposition, hydrothermal, microemulsion, and sol–gel, have been employed for MRNPC production, and a comprehensive comparison of these methods in terms of the key factors, advantages, and disadvantages is summarized in Table 1. Most MRNPCs involve more than one component, like the core–shell structure MRNPC comprising a magnetic core and outer shell with a photocatalyst, which usually requires multiple synthesis methods.[48] Researchers have the option to evaluate the desired characteristics of MRNPCs and opt for one or multiple synthesis methods for MRNPC fabrication.

Co-precipitation is the most commonly employed technique for producing iron oxides and spinel ferrites using two operating pathways. Pathway one entails the partial oxidation of $Fe(OH)_2$ suspensions using various oxidizing agents under alkaline conditions.[49] The second pathway is to age the mixtures of $Fe(OH)_2$ and $Fe(OH)_3$ in an alkaline solution, and finally obtain iron oxides.[50] The properties of the obtained materials are affected by the ratio of Fe^{2+}/Fe^{3+} in the solution, the reaction temperature, and the pH value.[51] This method possesses the advantages of easy operation, mild reaction conditions, and no specific equipment required, and it is promising for industrial applications because of the high product yield. However, particle nucleation is inevitable, leading to uncontrolled nanoparticle sizes and shapes.[52]

Thermal decomposition for magnetic material synthesis involves the chemical breakdown of the precursors (containing multi-component reactants with the necessary elements) in an organic solvent with stabilizing surfactants to produce uniform and monodisperse products.[53] The characteristics of the synthesized materials depend on the reaction temperature, duration, and the ratios of the starting reagents. Generally, this technique can produce nanomaterials with high crystallinity and purity due to the operational condition of high temperature. Additionally, it can control the sizes of the nanoparticles within the range of 3–20 nm.[50] Although thermal decomposition can be easily scaled up for nanomaterial production at an industrial level, limitations including high energy consumption, high-temperature requirements, and the expensive nature of metal–organic precursors hinder its widespread application.

The hydrothermal process can be used for the preparation of both magnetic materials and photocatalysts in MRNPCs. The method involves the nucleation of materials in a solution

Table 1 Comparison of synthesis methods

Synthesis method	Reaction condition		Shape control	Material production quantity	Advantages	Disadvantages
	Temp	Time				
Co-precipitation	20–100 °C	Minutes	Low	Low	(i) Simple synthesis route (ii) short synthesis time	(i) Poor shape control (ii) tend to agglomerate (iii) Wide size distribution
Thermal decomposition	100–350 °C	Hours to days	High	High	(i) Controllable size (ii) Narrow size distribution	(i) High temperature (ii) Complicated procedures (iii) Toxic organic reagents
Hydrothermal	100–250 °C	Hours	Medium	Medium	(i) No organic reagents (ii) Good magnetic responsiveness	(i) Time consuming (ii) High temperature and pressure
Microemulsion	20–50 °C	Hours	Medium	Low	(i) Conducive for modification of MNPs (ii) Reduces the aggregation	(i) Low yield (ii) Large amounts of solvent
Sol–gel	Room temperature	Hours	Medium	Medium	(i) No specialized equipment (ii) High purity (iii) Easy to mange	(i) Form byproduct that need separation (ii) The use of harmful chemical solvents

containing necessary elements under high pressure and temperature conditions for a long duration.[54] Compared with other techniques, the hydrothermal process can easily control the size and shape of the nanomaterials and even optimize their crystallinity and reactivity for the desired purpose by varying the reaction temperatures, process duration, and chemical use. Nevertheless, the method is only suitable for producing nanomaterials in the laboratory since the complex reaction conditions and energy-intensive features limit its scalability. Additionally, the method also suffers limitations of cost-intensive because of its slow reaction kinetics and stringent reaction conditions.[55]

The microemulsion method prepares nanoparticles by merging stable two-phase colloidal suspensions into one phase with the help of surfactants.[56,57] The method can effectively control nucleation, prevent agglomeration, and have low energy consumption, making it a very popular green synthesis method.[58] Moreover, the method also endows the produced nanomaterials with enhanced stability and high homogeneity because the confined reaction environment for nanomaterial growth provided by microemulsion can enhance the mechanistic strength of the products and prevent impurity incorporation.[59] However, the method faces the challenge of limited scalability due to being difficulty of maintaining a uniform and stable microemulsion system on a large scale. Even in the application of lab scale, this method also suffers high dosages of surfactants required, low production yield, and a restricted capacity for dissolving substances.[60]

The sol–gel method involves the conversion of liquid metallic precursors (sol) into the metal oxide solid gel network using chemical reactions. Subsequently, the final crystalline state is obtained with calcination.[61] The processes can be conducted at room temperature under mild conditions without the need for specific equipment. This approach allows for control of the morphology of the nanoparticles, which can obtain nanomaterials with desired morphologies, such as rods, spheres, and fibers, by adjusting the operational conditions, like reaction temperature, solvent composition, and precursor concentration.[62] In addition, the method is easy to scale up for the production of MRNPCs at an industrial level due to its considerable yielding efficiency. However, the utilization of hazardous chemical solvents and the generation of by-products requiring additional separation still hinder the practicability of the approach.[63] Future studies are suggested to develop non-toxic alternatives as solvents and reduce the generation of by-products, thus making the sol–gel method green for large-scale applications.

2.4 Separation of MRNPCs from treated water

Separation of photocatalysts from the treated solution is of great importance to the cost-effectiveness considerations of wastewater treatment, which involves the recovery of photocatalysts, product purity, and photocatalyst reuse. Filtration, gravity-induced sedimentation, and centrifugation are conventional approaches for achieving the recovery of photocatalysts from the treated wastewater. Filtration is the most effective method to separate photocatalysts and treated wastewater by using a filter medium, but the high cost of the consumable filter medium and the expensive filter facility hinder its application. Gravity-induced sedimentation relies on the difference in density between the photocatalyst and the water, which is suitable for separating large-size photocatalysts but not a good option for the recovery of nanophotocatalysts. Centrifugation, induced by centrifugal force, can efficiently and rapidly separate nanophotocatalysts, however, it is energy-intensive and not feasible for large wastewater volumes. Notably, the photocatalysts are separated along with other impurities from the treated water using these approaches, which adversely affects the quality of the collected photocatalysts and their further reuse.

Compared with conventional methods for the separation of photocatalysts, magnetic separation of MRNPCs from

treated water has emerged as a promising approach, offering the advantages of high separation efficiency and easy operation. In lab-scale experiments, after the photocatalytic reaction, a magnet is employed to provide an external magnetic field to separate the MRNPCs from the treated wastewater. Subsequently, the treated and purified wastewater can be discharged from the reactor, and thus the collected MRNPCs can be recycled. Afterwards, the recycled MRNPCs undergo washing procedures with clean water and organic agents to eliminate any residual contaminants or reaction byproducts. Finally, the recycled MRNPCs can be reintroduced into the wastewater treatment process, thereby minimizing the consumption of catalysts and reducing overall operational costs. Most importantly, magnetic separation has good selectivity for only collecting MRNPCs from the treated water and rejecting any impurities, ensuring the quality of the recovered MRNPCs for further reuse. Moreover, due to the characteristics of cost-effectiveness and ease of operation, the magnetic separation using a high-gradient magnetic separator has a promising potential that can be integrated into existing wastewater treatment systems, offering great benefits for large-scale industrial applications. Therefore, the easy magnetic separation of MRNPCs from treated water endows the technique with great promise for future industrial applications.

Nevertheless, current research mainly focuses on lab-scale investigation and the full-scale magnetic technique has not been developed yet, several challenges and considerations need to be addressed when employing magnetic separation of MRNPCs in realistic wastewater treatment, which are detailed and discussed in section 5.

3. Applications of MRNPCs in conventional photocatalysis

Most of the developed MRNPCs have been applied in conventional photocatalysis. Compared with other wastewater treatment techniques, photocatalysis using MRNPCs offers the merits of not requiring further reagents, low energy consumption, recyclability, and environmental friendliness. The mechanisms of photocatalysis using MRNPCs for organic pollutant removal are straightforward: under light illumination, the MRNPCs produce e^- and h^+ in the conduction band (CB) and valence band (VB), respectively (eqn (1)).[64] Later, the separated e^- and h^+ migrate to the material surface and react with water or oxygen molecules, resulting in the formation of hydroxyl radicals ($^{\bullet}OH$) and superoxide radicals ($O_2^{\bullet-}$) (eqn (2) and (3)).[65] Both $^{\bullet}OH$ and $O_2^{\bullet-}$ are reactive oxygen species (ROS) that have a strong oxidation capacity for degrading the pollutants into CO_2 and H_2O (eqn (4)).[66]

$$\text{MRNPCs} + h\nu \rightarrow \text{MRNPCs}\ (e^- + h^+) \quad (1)$$

$$h^+ + H_2O \rightarrow H^+ + {}^{\bullet}OH \quad (2)$$

$$e^- + O_2 \rightarrow O_2^{\bullet-} \quad (3)$$

$$\text{Pollutant} + {}^{\bullet}OH/O_2^{\bullet-} \rightarrow CO_2 + H_2O \quad (4)$$

In the beginning, pristine photocatalysts were integrated with magnetic materials, forming simple MRNPCs for wastewater treatment. However, these simple MRNPCs are far from satisfying the high efficiency required for pollutant removal. Along with the development of materials, various approaches, mainly element doping, heterojunction construction, and material functionalization, have been employed to modify the photocatalyst in MRNPCs, thereby improving the performance in pollutant degradation. Table 2 summarizes the details of MRNPCs in conventional photocatalysis, and the following sections introduce their current status and involved mechanisms.

3.1 MRNPCs with pristine photocatalysts

Combining pristine semiconductors with magnetic nanoparticles offers the simplest approach for MRNPC preparation. TiO_2, ZnO, and g-C_3N_4 are the most popular photocatalysts in this configuration due to their attractive features of low cost, ease of acquisition, high stability, and non-toxicity.[67–69] In general, Fe_3O_4 is applied as the magnetic material in these MRNPCs due to its outstanding magnetic properties. For example, Chang *et al.* prepared a Fe_3O_4/TiO_2 nanophotocatalyst with a core–shell structure, achieving complete removal of phenol under UV irradiation. Compared with TiO_2, Fe_3O_4/TiO_2 has a narrowed band gap of 1.39 eV and a M_s of 1.74 emu g^{-1}, and can be quickly separated from treated wastewater.[68] Similarly, ZnO/Fe_3O_4 was synthesized as MRNPC to eliminate different types of antibiotics. Less than 40% and 50% of the trimethoprim and erythromycin were degraded by ZnO/Fe_3O_4 in 4 h under UVA irradiation.[70] Unlike TiO_2 and ZnO, g-C_3N_4 has a band gap of 2.7 eV that can absorb a portion of visible light. A fluorinated Fe_3O_4/g-C_3N_4 sample was synthesized, with an exfoliation and porous structure, offering a high specific surface area of 242.71 $m^2\ g^{-1}$. Although the cylindrical photoreactor and immersed lamp enhanced the visible light utilization, less than 40% degradation of amoxicillin was observed in 2 hours.[71]

The MRNPCs using pristine photocatalysts offer an easily available strategy for material acquisition, however, the unsatisfactory performance greatly limits their practical potential. The above-mentioned MRNPCs suffer several limitations: (i) pristine photocatalysts have low solar conversion rates and therefore produce few charge carriers; (ii) many pristine photocatalysts have a limited absorption range that can only utilize a specific portion of the solar spectrum; and (iii) high charge recombination rate to reduce the available electrons and holes for pollutant degradation.[72,73] Researchers have made significant efforts to mitigate these limitations by exploring novel MRNPCs using varying modification approaches, as shown in the below sections.

Table 2 Application of MRNPC in conventional photocatalysis

MNPC	Synthesis method	Modification method	Target pollutant	Working conditions: Pollutant dose	Catalyst dose	Light source	Time (min)	M_s (emu g^{-1})	Removal efficiency	Ref.
Fe_3O_4/TiO_2	Co-precipitation	N/A	Phenol	100 mg L^{-1}	3 g L^{-1}	UV	150	1.74	100%	68
$ZnFe_2O_4/SiO_2/TiO_2$	Co-precipitation and sol–gel method	Type II heterojunction	Etodolac	15 mg L^{-1}	2 g L^{-1}	UV–VIS	20	25	100%	69
Fe_3O_4/ZnO	Co-precipitation	N/A	Sulfamethoxazole trimethoprim erythromycin roxithromycin	0.1 mg L^{-1}	0.2 g L^{-1}	UVA	240	4.3	>90%	70
$Fe_3O_4/g\text{-}C_3N_4$	Hydrothermal method and thermal decomposition	N/A	Amoxicillin	90 mg L^{-1}	1 g L^{-1}	VIS, UV	120	N/A	~86%	71
$N\text{-}TiO_2@SiO_2@Fe_3O_4$	Co-precipitation and sol–gel method	Non-metal ion doping	Ibuprofen benzophenone-3	2 mg L^{-1}	1 g L^{-1}	VIS	300	8.96	$P_{[IBU]}$ = 94%, $P_{[BZP\text{-}3]}$ = 93%	79
Fe_3O_4/graphene/S-doped $g\text{-}C_3N_4$	Co-precipitation and thermal decomposition	Non-metal ion doping	Ranitidine	5 mg L^{-1}	1 g L^{-1}	VIS	60	N/A	100%	80
$I\text{-}TiO_2/SiO_2/Fe_3O_4$	Microemulsion and hydrothermal method	Non-metal ion doping	Phenol	16.7 mg L^{-1}	1 g L^{-1}	VIS	240	1.18	73.5%	81
$\gamma\text{-}Fe_2O_3@SiO_2@Ce\text{-}doped\text{-}TiO_2$	Sol–gel method	Metal ion doping	Rhodamine B	48 mg L^{-1}	1 g L^{-1}	UV–VIS	180	5.8	88%	83
$\gamma\text{-}Fe_2O_3@SiO_2@TiO_2\text{–}Ag$	Sol–gel process and hydrothermal method	Metal ion doping	Methyl orange	30 mg L^{-1}	1 g L^{-1}	UV	60	N/A	84%	84
Graphene oxide-Ce-TiO_2	Sol–gel method	Metal ion doping	Tetracyclines	25 mg L^{-1}	0.5 g L^{-1}	VIS	60	N/A	82.9%	86
La/N co-doped $TiO_2/SrFe_2O_4$/diatomite	Sol–gel method	Metal & non-metal ions co-doping	Oxytetracycline	10 mg L^{-1}	2.0 g L^{-1}	VIS	150	0.89	95.5%	89
TiO_2/Fe_2O_3	Ultrasonic-assisted sol–gel method	Type II heterojunction	Paracetamol	50 mg L^{-1}	0.1 g L^{-1}	UV–VIS	90	20.82	75%	96
$Sn_3O_4/SnFe_2O_4$	Hydrothermal method	Type II heterojunction	Ciprofloxacin	10 mg L^{-1}	0.5 g L^{-1}	VIS	120	10	57%	97
$ZnFe_2O_4@CuFe_2O_4@SiO_2$	Co-precipitation	Type II heterojunction	Methylene blue	32 mg L^{-1}	0.6 g L^{-1}	VIS	70	0.806	98.6%	98
$TiO_2/Fe_3O_4/CoWO_4$	Co-precipitation	p–n heterojunction	Rhodamine B	4.8 mg L^{-1}	—	VIS	330	12.5	99.1%	100
$Fe_3O_4/ZnO/NiWO_4$	Co-precipitation	p–n heterojunction	Rhodamine B	4.8 mg L^{-1}	0.4 g L^{-1}	VIS	300	5.88	97.9%	101
$TACN/TiO_2/Fe_3O_4@SiO_2$	Sol–gel and hydrothermal methods	Z-scheme heterojunction	Ibuprofen	2 mg L^{-1}	1 g L^{-1}	VIS	60	8	100%	103
$g\text{-}C_3N_4/TiO_2/\alpha\text{-}Fe_2O_3$	Thermal decomposition and hydrothermal method	Z-scheme heterojunction	Rhodamine B	50 mg L^{-1}	0.03 g L^{-1}	VIS	50	N/A	95.7%	104
$Fe_3O_4/g\text{-}C_3N_4/MoO_3$	Thermal decomposition	Carbon material functionalization	Tetracycline	40 mg L^{-1}	2 g L^{-1}	VIS	120	26.3	84%	105
$ZnO/Fe_3O_4/g\text{-}C_3N_4$	Co-precipitation and sol–gel method	Carbon material functionalization	Pantoprazole	30 mg L^{-1}	0.8 g L^{-1}	VIS	90	16.16	97%	106
$Fe_3O_4/CdS/g\text{-}C_3N_4$	Co-precipitation and thermal decomposition	Carbon material functionalization	Ciprofloxacin	20 mg L^{-1}	1 g L^{-1}	VIS	180	N/A	81%	107
Fe_3O_4/reduced graphene oxide	Co-precipitation	Carbon material functionalization	Carbamazepine	—	0.5 g L^{-1}	VIS	180	45.7	98.7%	109

Table 2 (continued)

MNPC	Synthesis method	Modification method	Target pollutant	Working conditions				M_s (emu g^{-1})	Removal efficiency	Ref.
				Pollutant dose	Catalyst dose	Light source	Time (min)			
Fe_3O_4@SiO_2@$BiFeO_3$/rGO	Hydrothermal method	Carbon material functionalization	Methylene blue, rhodamine B	5 mg L^{-1}	1 g L^{-1}	VIS	90	20.3	$P_{[MB]}$ = 98.2%, $P_{[RhB]}$ = 95.6%	110
$ZnFe_2O_4$@methyl cellulose	Microwave-assisted method	Biomaterial functionalization	Metronidazole	5 mg L^{-1}	1 g L^{-1}	UV-C	100	28.05	92.65%	114
$CuFe_2O_4$@methyl cellulose	Microwave-assisted method	Biomaterial functionalization	Ciprofloxacin	3 mg L^{-1}	0.67 g L^{-1}	UV	90	17.44	80.7%	115
Fe_3O_4/BiOBr/BC	Microemulsion	Biomaterial functionalization	Carbamazepine	10 mg L^{-1}	1 g L^{-1}	VIS	180	5.2	95.5%	118
BC@$ZnFe_2O_4$/BiOBr	Hydrothermal method	Biomaterial functionalization	Ciprofloxacin	15 mg L^{-1}	0.5 g L^{-1}	UV-VIS	60	8.57	84%	119
Bi_2WO_6/Fe_3O_4/BC	Hydrothermal method	Biomaterial functionalization	Ofloxacin, ciprofloxacin	10 mg L^{-1}	0.4 g L^{-1}	LED	30	6.2	100%	120
MIL-100(Fe)@Fe_3O_4/CA	Microemulsion and co-precipitation	MOF functionalization	Tetracycline	10 mg L^{-1}	0.2 g L^{-1}	VIS	150	45	85%	122
Cu_2O/Fe_3O_4/MIL-101(Fe)	Hydrothermal method and co-precipitation	MOF functionalization	Ciprofloxacin	20 mg L^{-1}	0.5 g L^{-1}	VIS	120	25.7	99.2%	123

Note: M_s is the saturation magnetism of the MRNPCs.

3.2 MRNPCs modified with element doping

Element doping has been studied to adjust the band gap and other features of photocatalysts.[74] The activity of an element-doped photocatalyst is affected by the nature of the dopant. Generally, non-metals are preferred in element doping over metals because they are more affordable and easier to acquire.[75] As shown in Fig. 3a, compared with a pristine photocatalyst, the doping of non-metal ions reconstructs the valence band of the material and moves it upwards, leading to a narrowed band gap.[76–78] As a result, the utilization of the solar spectrum is improved because the light adsorption range of the modified photocatalysts is greatly extended, thereby resulting in an enhanced performance.

Nitrogen is favored in non-metals doping as it has a similar atomic structure to oxygen that can be employed to replace oxygen in the lattice of TiO_2. Kumar *et al.* synthesized N-TiO_2@SiO_2@Fe_3O_4 (NTSF) for the degradation of ibuprofen (IBU) and benzophenone-3 (BZP-3). The introduction of nitrogen dopants altered TiO_2's electronic band structure due to the formation of a novel N 2p band, which led to a reduced TiO_2 band gap. Consequently, more than 90% of IBU and BZP-3 were degraded within 5 hours of exposure to energy-saving LED.[79] Differing from nitrogen doping, sulfur doping not only provides band gap tuning but also promotes composite conductivity. Fe_3O_4/graphene/S-doped g-C_3N_4 (Fe_3O_4/GE/SCN) was developed for the decontamination of ranitidine, and it was found S atoms preferentially replaced the large electronegative N atoms in g-C_3N_4, leading to a narrowed band gap and improved charge transfer ability (Fig. 3b and c).[80] The synergistic effect increased the generation of charge carriers and restrained the recombination, allowing the complete degradation of ranitidine in 1 hour. Furthermore, the reactive species scavenging tests revealed that the contributions of radicals for ranitidine degradation followed the sequence of $O_2^{\bullet-} > h^+ > {}^{\bullet}OH$ (Fig. 3d). As shown, in Fig. 3e, Fe_3O_4/GE/SCN achieved promoted separation of photogenerated electrons and holes under visible light, where electrons can oxidize oxygen to produce $O_2^{\bullet-}$ or simulate Fe^{2+}/Fe^{3+} for $O_2^{\bullet-}$ generation, and holes can directly degrade ranitidine or oxidize water to produce ${}^{\bullet}OH$ for ranitidine removal. Similarly, iodine doping served the same role as sulfur in MRNPC. He *et al.* synthesized an iodine-doped TiO_2/SiO_2/Fe_3O_4 (ITSF) for phenol degradation. The extended visible light region achieved by ITSF was attributed to the atomic configurations of I–O–I and I–O–Ti. In addition, I ions promoted the transfer of photogenerated electrons to improve charge separation. In addition, I ions promoted the transfer of photogenerated electrons to improve charge separation.[81]

As shown in Fig. 3a, doping metal ions in MRNPCs results in greater photocatalytic activity compared to non-metal ions due to: (i) easier electron excitation by shifting the band state nearer to the conduction band (CB) or valence band (VB); (ii) reduced recombination of photogenerated charge carriers through electron trapping from their original state; and (iii)

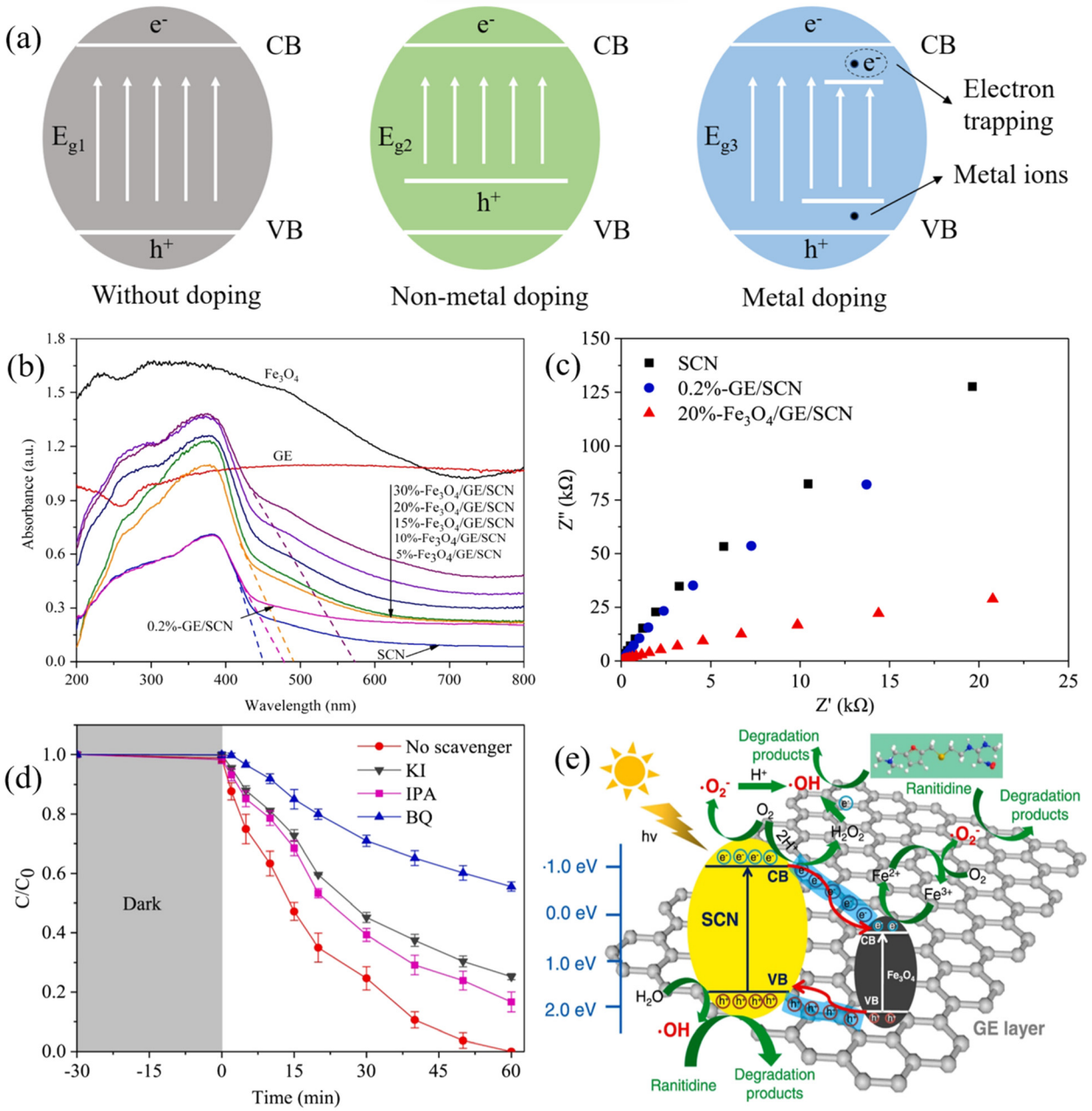

Fig. 3 (a) Schematic diagram showing the band gap energies of photocatalysts without doping, non-metal doping, and metal doping; (b) UV-vis light adsorption and (c) EIS Nyquist plots of Fe_3O_4/graphene/S-doped g-C_3N_4 (Fe_3O_4/GE/SCN) and other synthesized materials; (d) reactive species scavenging texts for the degradation of ranitidine (using KI, IPA, and BQ as the quenchers of h^+, $^{\cdot}OH$, and $O_2^{\cdot-}$); (e) the proposed mechanisms of ranitidine degradation by Fe_3O_4/GE/SCN under visible light illumination. Reproduced from ref. 80 with permission from Elsevier, copyright 2021.

improved conductivity of MRNPCs to facilitate the transfer of charge carriers to the material surface.

The introduction of transition metals of Fe, Co, Ni *via in situ* synthesis provides improvement of ferromagnetic property. The magnetic products also exhibit outstanding photoelectric properties and stability in treating organic pollutants.[82] Ce and Ag are the common metals for doping in MRNPCs because of their characteristics of excellent electron trapping ability and good conductivity.[83,84] In addition, the doping of Ce also affects the catalyst's growth, making it easier to produce small particles with a larger surface area.[85] For example, magnetic graphene oxide-loaded Ce-doped Titania (MGO-Ce-TiO_2) was prepared through a sol–gel method, achieving 82.92% removal of phenol in 1 hour under visible light due to the Ce doping trapping electrons for better charge separation and increased material surface area. When the mass ratio of Ce–TiO_2 in the MRNCP increased from 0 to 20%, the specific surface area increased from 50.39 to 203.71 $m^2\ g^{-1}$.[86] Additionally, He *et al.* reported that Ce doping in γ-Fe_2O_3@SiO_2@Ce-doped-TiO_2 can extend the light

adsorption range of the material. Ce doping caused the redshift on the absorption edge, which was ascribed to the stimulated electron transition, either from the Ce–TiO_2 VB or Ce_2O_3 ground state, towards the Ce 4f energy level. As a result, the material exhibited improved performance under visible light and 88% of rhodamine B (RhB) can be removed in 3 h.[83] On the other hand, γ-Fe_2O_3@SiO_2@TiO_2–Ag was prepared using sol–gel and hydrothermal methods. After 1 hour of UV radiation, more than 80% of the methyl orange was eliminated by the nanocomposite compared to 49% using pure TiO_2. The PL spectra indicated that the inclusion of silver can enhance charge separation by trapping photogenerated electrons, consequently improving photoactivity.[84]

Co-doping with both metallic and non-metallic elements represents a promising approach for producing MRNPCs with enhanced performance and good stability.[87,88] For instance, Chen *et al.* facilitated a La/N co-doped TiO_2/$SrFe_2O_4$/diatomite (La/N-TiO_2/Dt) for oxytetracycline (OTC) degradation. More than 90% OTC was removed by La/N-TiO_2/Dt in 2.5 h under visible light, exhibiting improved performance compared with samples with single elemental doping. The co-doping of lanthanum and nitrogen endowed the catalyst with the advantages of both metal doping and non-metal doping.[89]

However, some negative effects of element doping are inevitable. As for non-metal doping, the synthesis method requires high temperatures and complex routes as it involves the intercalation of doped ions into the lattice of the MRNPCs.[90] As a result, non-metal doping represents a laborious and energy-intensive approach. On the other hand, concerns associated with metal doping are: (i) MRNPCs modified by metal ion doping are unstable and may cause secondary pollution from metal leaching; (ii) transition metals are highly reactive but toxic; and (iii) most metal doping involves the use of noble ions, increasing the cost of MRNPC fabrication.[91,92] In light of the aforementioned challenges, researchers should explore novel approaches to simplify the synthesis procedure for non-metal doping and mitigate the utilization of noble metals by seeking highly reactive non-noble metal ions as alternatives.

3.3 MRNPCs modified with heterojunction construction

A heterojunction refers to the interfacial configuration between two distinct semiconductors or metal layers.[93] One semiconductor grows epitaxially over another, creating elaborate epitaxial bonding surfaces that accelerate electron migration, thus reducing the tendency for charge recombination. By constructing heterojunctions, the composite also expands the light absorption to a higher wavelength zone.[94,95] Conventional heterojunctions can be categorized as type-I, type-II, and type-III, according to their distinct band alignments.[93] Due to the significantly reduced redox performance and broken gaps, type-I and type-III heterojunctions are rarely studied. As for type-II heterojunctions, the semiconductor S1 has higher VB and CB energy levels than those of semiconductor S2 (Fig. 4a). As a result, electrons move to the CB of S1, and holes travel to the VB of S2, leading to spatial charge separation.

In light of this, Abdel-Wahab *et al.* developed the type-II heterojunction TiO_2/Fe_2O_3 MRNPC for the degradation of paracetamol, which achieved high photocatalytic activity due to the heterojunction structure enhanced the light absorption intensity of the material and benefited the separation of e^-/h^+ pairs.[96] Similarly, a typical type-II heterojunction-based catalyst Sn_3O_4/$SnFe_2O_4$ (SN/SFO) was prepared for ciprofloxacin (CIP) removal. The sufficient number of pores in flower-like SN/SFO also led to a larger exposed surface area to facilitate CIP degradation (Fig. 4b). Moreover, the tight interfacial contact between SN and SFO also facilitated efficient charge transfer (Fig. 4c). Consequently, SN/SFO showed the highest CIP degradation efficiency of 57% in 2 h compared to SN or SFO.[97] In a specific case, two spinel ferrites were used to form a ternary type-II-based $ZnFe_2O_4$@$CuFe_2O_4$@SiO_2 heterojunction. The composites showed reduced charge recombination compared to $ZnFe_2O_4$@$CuFe_2O_4$, $ZnFe_2O_4$, and $CuFe_2O_4$ according to the PL spectra and 98.6% Methylene Blue (MB) degradation in 70 minutes under visible light.[98] Li *et al.* synthesized the magnetic sphere Fe_3O_4/Ag/m (TiO_2–ZrO_2) with a sandwich and core–shell structure using Ag nanoparticles as an interim layer that protect the photocatalyst from thermal damage, and that exhibits rapid 98% Cr(VI) reduction after 30 min of Hg lamp irradiation.[99]

Nonetheless, the migration of electrons and holes in a type-II heterojunction is impeded by the electrostatic repulsion. The p–n heterojunction is regarded as an advanced type-II heterojunction because of a similar mechanism, which can appropriately address the limitations of the type-II heterojunction. When p-type and n-type semiconductors are combined, the p–n heterojunction exhibits efficient photocatalytic properties because the e^-/h^+ diffusion near the p–n interface forms an internal electric field that can accelerate electron migration (Fig. 4a).

Based on this principle, Feizpoor *et al.* fabricated a TiO_2/Fe_3O_4/$CoWO_4$ p–n heterojunction that demonstrated a RhB degradation efficiency of 99.1% in 330 minutes of visible light irradiation. Under light illumination, p-type $CoWO_4$ experienced a rise in CB and VB energy levels, while n-type TiO_2 experienced a decrease until equilibrium was reached. This state of balance established an electric field that promoted charge separation.[100] Similarly, a 40%-Fe_3O_4/ZnO/$NiWO_4$ was reported to degrade RhB by 97.9% in 300 minutes. The formed p–n heterojunction between $NiWO_4$ and ZnO played a major role in the separation and transfer of photogenerated charge carriers, achieving a remarkable promotion in degradation performance. In addition, the prepared MRNPC had a high magnetization value (12.5 emu g^{-1}).[101]

Both type II and p–n heterojunctions suffer a reduction of redox capacity since both oxidation and reduction reactions

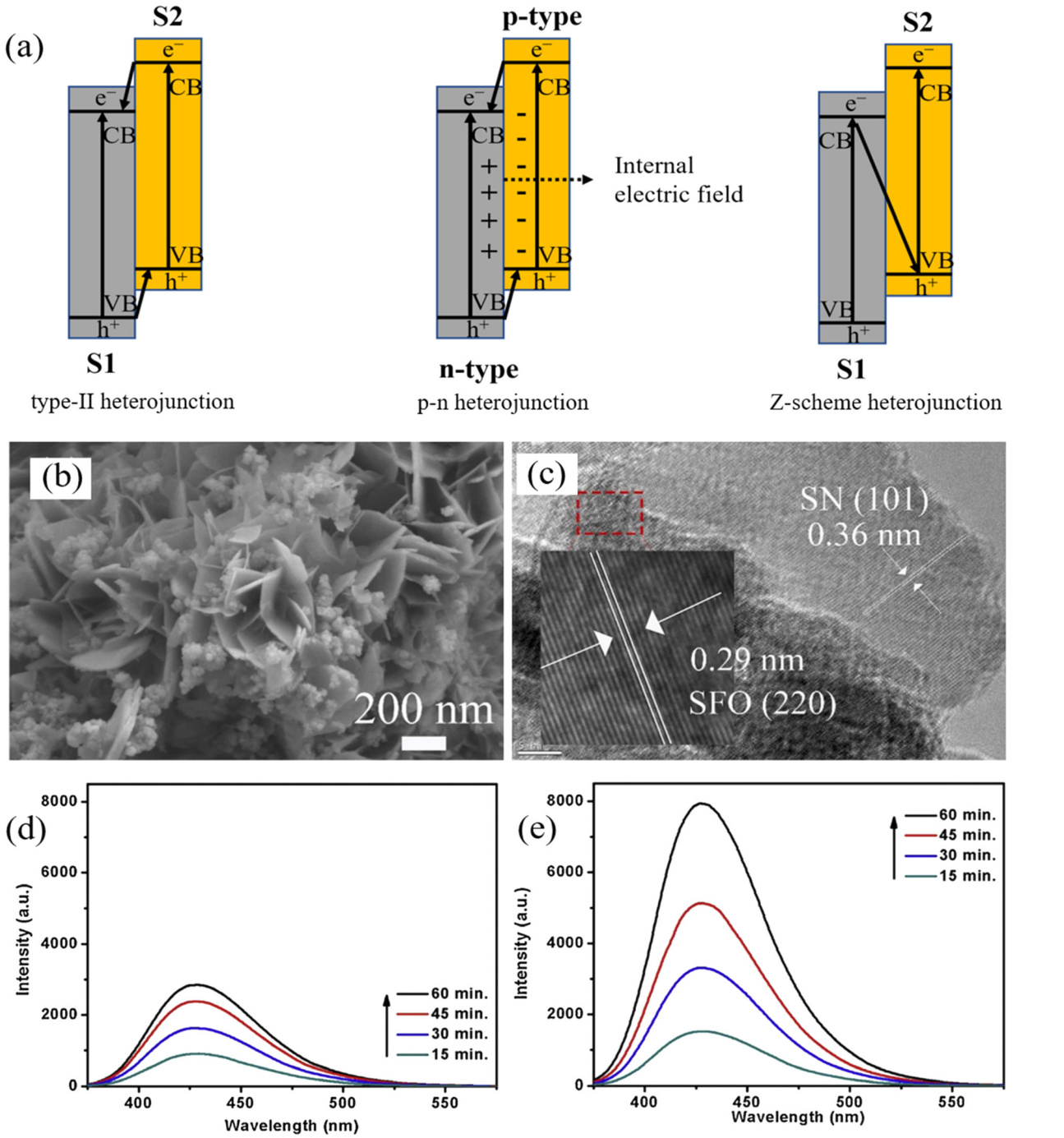

Fig. 4 (a) Mechanisms of charge transfer in type-II, p–n, and Z-scheme heterojunction; (b) SEM image and (c) HRTEM image of $Sn_3O_4/SnFe_2O_4$–25% (SN/SFO-25%) composite. Reproduced from ref. 97 with permission from Elsevier, copyright 2022. PL emission spectra of (d) $TiO_2/Fe_3O_4@SiO_2$ nanophotocatalysts, and (e) $TACN/TiO_2/Fe_3O_4@SiO_2$ heterojunction nanophotocatalyst to show the production of $^{\cdot}OH$ using terephthalic acid as the chemical probe. Reproduced from ref. 103 with permission from Elsevier, copyright 2020.

occur on the semiconductor surface with lower oxidation and reduction potential. The Z-scheme heterojunctions have been developed to maintain high oxidation and reduction capabilities, addressing the above-mentioned limitations. As shown in Fig. 4a, in a typical Z-scheme heterojunction, e^-/h^+ pairs are transferred and built up on the semiconductor with a higher redox potential by an electron mediator channel or the electron pair pathway.[102] In the meantime, the electrostatic attraction between e^- and h^+ also benefits the charge migration in the Z-scheme heterojunction.

To this end, Kumar *et al.* reported a magnetically recyclable Z-scheme $TACN/TiO_2/Fe_3O_4@SiO_2$ heterojunction for IBU removal, achieving 100% degradation in 1 hour under visible light irradiation. As shown in Fig. 4d and e,

compared with $TiO_2/Fe_3O_4@SiO_2$, $TACN/TiO_2/Fe_3O_4@SiO_2$ achieved high yield of $^{\bullet}OH$, indicating the successful construction of a Z-scheme heterojunction that led to a faster electron transfer and a low charge recombination.[103] Furthermore, a Z-scheme $g\text{-}C_3N_4/TiO_2/\alpha\text{-}Fe_2O_3$ heterojunction was reported to remove 95.7% of RhB within 50 minutes under visible light. Notably, in the composite, $\alpha\text{-}Fe_2O_3$ acts not only as a magnetic core (6.84 emu g^{-1}) for easy separation but also as a redox intermediary for electron transfer.[104] A similar role of Fe_3O_4 was found by He *et al.*[105] who developed innovative visible-light-driven Z-scheme $Fe_3O_4/g\text{-}C_3N_4/MoO_3$. The Fe_3O_4 electron mediator regulated charge transfer to ensure the retention of potent redox properties of e^- and h^+ for pollutant degradation.

3.4 MRNPCs modified with hybrid functionalization

To improve the photocatalytic activity of MRNPCs, different materials, including carbon materials, biomaterials, and metal–organic frameworks (MOFs) have been introduced to functionalize MRNPCs. The applications of these hybrids in conventional photocatalysis and their pros and cons are discussed below.

(1) Carbon material functionalization. Carbon-based materials are applied as a support material to fabricate MRNPCs due to their easy acquisition, high chemical stability, and excellent conductivity. These carbonaceous supports can work as the matrices for fast charge carrier transfer, prevent agglomeration of MRNPCs, and provide a high surface area to increase reactive sites. In addition, the introduction of carbon-based material enhances photostability, allowing long-term reusability.

Graphite carbon nitride ($g\text{-}C_3N_4$) is a visible-light-driven, two-dimensional, and metal-free catalyst, which has attracted widespread interest due to its narrow band gap and good chemical stability. For example, a $ZnO/Fe_3O_4/g\text{-}C_3N_4$ nanocomposites was prepared to remove pantoprazole, achieving a degradation efficiency of 97% in 1.5 h. The nanohybrids $ZnO/Fe_3O_4/g\text{-}C_3N_4$ had a band gap of 2.48 eV, lower than pristine ZnO (3.03 eV) and $g\text{-}C_3N_4$ (2.72 eV). Furthermore, the PL spectrum showed that the $ZnO/Fe_3O_4/g\text{-}C_3N_4$ has a lower peak intensity than ZnO/Fe_3O_4, indicating that the introduction of $g\text{-}C_3N_4$ greatly reduced charge recombination.[106] Likewise, Zhang *et al.* synthesized $Fe_3O_4/CdS/g\text{-}C_3N_4$ (FCN) for the effective degradation of CIP. The incorporation of $g\text{-}C_3N_4$ regulated the charge transfer direction and reduced the photo corrosion of CdS. FCN also exhibited super-paramagnetism and could be separated from the dispersed suspension in 90 s.[107]

Apart from $g\text{-}C_3N_4$, graphene oxide (GO) is also a promising two-dimensional carbon material to functionalize MRNPCs. It possesses several unique characteristics, such as outstanding chemical and physical properties, large surface area, and high conductivity.[108] Based on these benefits, the Fe_3O_4/reduced-GO (rGO) was fabricated to degrade carbamazepine, and rGO was found to minimize charge carrier recombination and offer a large surface area to enhance adsorption capacity and increase reaction sites. These improvements led to 98.7% of carbamazepine degradation in 3 hours under visible light, while maintaining a high M_s (45.7 emu g^{-1}).[109] Moreover, Su *et al.* developed $Fe_3O_4@SiO_2@BiFeO_3/rGO$ using the hydrothermal method, which achieved excellent photocatalytic activity with 98.2% degradation for tetracycline hydrochloride and 95.6% removal for CIP within 90 min. The introduction of GO reduced the band gap of $BiFeO_3$ from 2.5 eV to 1.91 eV, manifested the transfer of photoinduced carriers, and increased the surface area from 99.93 m^2 g^{-1} to 139.26 m^2 g^{-1}.[110]

However, there are concerns raised regarding carbon material. First, excess carbon material would mask the light adsorption and reaction sites of photocatalysts, leading to a decreased performance. Moztahida found that 20w%-rGO/Fe_3O_4 (20w%-rGF) had a decreased removal rate than 10w%-rGF because the carbon material itself has no catalytic activity.[109] The same phenomenon can also be seen in Zhang *et al.*'s study.[107] Second, carbon materials easily leach from the hybrids due to the poor compatibility between carbon materials of other inorganic components in MRNPCs. Ahmed *et al.* reported that the presence of GO and rGO in aquatic environments can pose negative effects on the microbes. Therefore, it is suggested that researchers should minimize the number of carbon materials in MRNPC and develop new synthesis methods to improve the compatibility between carbon materials and inorganic components.[111]

(2) Biomaterial functionalization. Methylcellulose (MC), an eEnvironmental-friendly biomaterial, can functionalize MRNPCs to increase their specific surface areas and deter aggregation.[112,113] $ZnFe_2O_4@MC$ was reported for degrading metronidazole, achieving a better efficiency of 93.87% on metronidazole degradation than $ZnFe_2O_4$ alone (79.98%). Apart from enlarging the material's surface area, the introduction of MC benefited the mass transfer electrostatic attraction between the pollutant and material through electrostatic attraction.[114] Moreover, Tamaddon *et al.* synthesized a similar bio-magnetic nanophotocatalyst $CuFe_2O_4@MC$ for CIP degradation, resulting in a high CIP removal efficiency of 80.7% in 90 minutes under UV light. When in contact with a pollutant, the methoxy group on MC stimulated the production of additional charge carriers, thus boosting the degradation.[115]

Biochar (BC) is a green and eco-friendly biomaterial that can be made from various sources such as agricultural waste, industrial waste, and woody material.[116] The use of BC for the production of MRNPCs has become widespread because of its good recyclability, low cost, and wide compatibility properties. Additionally, the presence of oxygen-containing functional groups on the surface of BC can also promote the adsorption of organic pollutants for better degradation.[117] In view of these, Li's group coupled $Fe_3O_4/BiOBr$ on reed straw biochar to form $Fe_3O_4/BiOBr/BC$, which showed a 41.8%

increase in surface area compared to Fe_3O_4/BiOBr and maintained a good magnetism (M_s value = 5.2 emu g^{-1}). As a result, Fe_3O_4/BiOBr/BC exhibited better performance for CBZ degradation (95.51% removal) under irradiation from an energy-saving LED.[118] Additionally, BC@$ZnFe_2O_4$/BiOBr was developed for CIP degradation. The transient photocurrent analysis and EIS showed that the BC@$ZnFe_2O_4$/BiOBr has a higher photocurrent and a lower electric resistance than $ZnFe_2O_4$/BiOBr because BC served as an electron mediator for better charge separation. Consequently, the nanocomposite presented an 84% removal efficiency of CIP in 1 h under visible light.[119] Furthermore, the flower-like Bi_2WO_6/Fe_3O_4 has also been coupled on BC to form Bi_2WO_6/Fe_3O_4/BC for CIP degradation. The SEM images showed that Bi_2WO_6/Fe_3O_4 particles were tightly attached to the rough surface of BC, thus the agglomeration was inhibited. More than 95% CIP was removed in 30 min of LED light irradiation. However, the decreased crystallinity led to a reduced performance after five cycles.[120]

The functionalization of MRNPCs using biomaterials represents a green and sustainable method. Firstly, biomaterials with the desired characteristics can be synthesized from different sources and selected from local surplus waste, effectively turning waste into a recyclable support material.[116] Secondly, biomaterials can be further modified to prevent metal leaching and photo-corrosion of MRNPCs while promoting their porosity and functionality for enhanced performance. Additionally, the used material can be regenerated using steam activation to transfer by-products into gaseous products and unblock the pores, thereby ensuring the long-term performance of the material.[121]

(3) MOF functionalization. MOFs are a group of crystalline materials formed by metal clusters and organic ligands, which possess a large surface area and a pore structure. Owing to their tunable structure, MOFs can be functionalized or coupled with other materials to serve as photocatalysts with outstanding performance. For example, MIL-101(Fe) with a high porosity and low resistance was employed to support the Cu_2O/Fe_3O_4 nanocomposite. The synthesized Cu_2O/Fe_3O_4/MIL-101(Fe) has an extremely narrow band gap of 1.0 eV and resulted in 99% removal of CIP in 2 h under visible light irradiation. The material also exhibited excellent stability with only 6% reduction in degradation efficiency after 5 continuous cycles.[122] MOF can also serve as a magnetic material in MRNPC through proper modification. He *et al.* developed a heat-treating method at 350 °C to magnetize M-MIL-101(Fe) and coupled it with TiO_2 to obtain M-MIL-101(Fe)/TiO_2, which achieved more than 95% of tetracycline (TC) degradation within 30 min under solar light. The material exhibits low stability, as evidenced by certain damage in the crystallinity and structure of M-MIL-101(Fe)/TiO_2 after 5 runs of utilization.[123] Recently, Yang *et al.* developed La–$ZnFe_2O_4$@Fe_3O_4@carbon with Fe/Zn MOF as a dopant source using a simple absorption–pyrolysis method. The magnetic hybrid composite possesses effective removal of mycotoxins from water: after 30 min of visible light irradiation (≥420 nm), ~98% of aflatoxin B1, patulin, and zearalenone (5 mg L^{-1}) are mineralized, with high performance and structural stability after cycles of treatment.[124]

A major issue in the application of MOFs in MRNPC is the poor stability of MOFs under harsh conditions, such as exposure to acids/bases and anions, which may lead to structural collapse.[123] Moreover, the stability of MOFs is also affected by the metal ions and ligands used to construct the framework and the surface hydrophobicity.[124] Therefore, for the development of MRNPCs *via* MOF functionalization, researchers should pay attention to improving the stability of the employed MOFs.

4. Photocatalysis-assisted processes using MRNPCs

The performance of conventional photocatalysis mainly depends on the properties of MRNPCs. To this end, various synthesis methods and numerous modification technologies have been developed to enhance the performance of photocatalysts, necessitating intricate procedures. Nevertheless, the limited stability of composite materials, challenges associated with synthesis, and the inherent drawbacks of conventional photocatalysis impose significant constraints on its practical application. To address these limitations and improve the use of photo-generated electrons, photocatalysis has been integrated with complementary techniques, leading to the development of combined processes, such as photocatalytic Fenton-like processes, photocatalytic sulfate radical-based AOPs, photocatalytic ozonation, and sono-photocatalysis. In this section, these combined processes using MRNPCs are reviewed, highlighting their potential to overcome the drawbacks of conventional photocatalysis.

4.1 Photocatalytic Fenton-like processes

Researchers have integrated photocatalysis and the Fenton reaction, devising a unique technique for treating wastewater, namely the photocatalytic Fenton-like process. Compared to the single-generation pathway of $^{\bullet}OH$ in photocatalysis, the photocatalytic Fenton-like processes using MRNPCs provide multiple routes for $^{\bullet}OH$ generation with the addition of H_2O_2 to enhance the efficiency of pollutant degradation.[125] Compared with the conventional Fenton process, the combined process utilizes solid iron-based MRNPCs instead of iron salts, avoiding iron sludge and follow-up processing. In addition, the MRNPCs activate H_2O_2 through charge carriers and surface active sites, thus hindering the loss of iron ions and enabling a broad range of working pH values. Since MRNPCs can be easily recycled and reused, the photocatalytic Fenton-like processes using MRNPCs are more cost-effective and widely applicable compared with

conventional Fenton processes. For a comprehensive sketch, MRNPCs used in photocatalytic Fenton-like processes are summarized in Table 3.

Fig. 5a illustrates the mechanism of the photocatalytic Fenton-like process using MRNPCs. Upon light illumination, H_2O_2 can be activated by the photogenerated electrons produced by MRNPCs to produce $^{\bullet}OH$ (eqn (5)).[139] Due to the capture of electrons by H_2O_2, more photogenerated holes can be separated to produce $^{\bullet}OH$ for pollutant degradation (eqn (2)). Further, Fe^{2+} in MRNPCs activates H_2O_2 to generate $^{\bullet}OH$ and form Fe^{3+} as a chain initiation reaction (eqn (6)). Then, Fe^{3+} further reacts with H_2O_2 to generate Fe^{2+} as the chain termination reaction (eqn (7)).[130] Moreover, e^- can also reduce Fe^{3+} into Fe^{2+} to facilitate the Fe^{2+}/Fe^{3+} cycle (eqn (8)).[35] The $O_2^{\bullet-}$ is generated through oxygen reaction by electrons (eqn (3)). Both $^{\bullet}OH$ and $O_2^{\bullet-}$ can degrade the pollutants into CO_2 and H_2O (eqn (4)). The photogenerated electrons can reduce Fe^{3+} to Fe^{2+}, facilitating Fe^{2+}/Fe^{3+} cycles for sustained $^{\bullet}OH$ production.[140]

$$H_2O_2 + e^- \rightarrow {}^{\bullet}OH + OH^- \quad (5)$$

$$Fe^{2+} + H_2O_2 \rightarrow Fe^{3+} + HO^- + {}^{\bullet}OH \quad (6)$$

$$Fe^{3+} + H_2O_2 \rightarrow Fe^{2+} + H^+ + HO_2^{\bullet} \quad (7)$$

$$Fe^{3+} + e^- \rightarrow Fe^{2+} \quad (8)$$

In the photocatalytic Fenton-like process, Fe_3O_4 is more effective than Fe_2O_3 because it has both Fe^{2+} and Fe^{3+} ions in octahedral sites and Fe^{2+} has a higher reaction rate with H_2O_2 for $^{\bullet}OH$ production than that of Fe^{3+}.[141] In general, Fe_3O_4 has a high magnetism but a weak photocatalytic ability. For example, a Fe_3O_4–GO MRNPC was synthesized through a combination of co-precipitation and hydrothermal techniques for H_2O_2 activation. Due to the relatively low photocatalytic activity and high charge recombination of Fe_3O_4, the Fe_3O_4–GO/H_2O_2 exhibited a relatively average performance in phenol removal.[128]

Thus, Fe_3O_4 is often combined with other semiconductors to form MRNPCs for the photocatalytic Fenton-like process, achieving synergistic effects in H_2O_2 activation due to the close interaction between Fe_3O_4 and the photocatalysts. For instance, the use of Fe_3O_4@rGO@AgI exhibited a significantly improved performance in phenol degradation compared to Fe_3O_4 and Fe_3O_4@rGO, which was ascribed to the abundant generation of electrons and their rapid transportation.[126] Similarly, Fe_3O_4 and TiO_2 nanoparticles were co-assembled on GO, forming TiO_2–GO–Fe_3O_4 composites to activate H_2O_2 for amoxicillin degradation. Such a configuration endowed the material with magnetism and high visible light response activity, evidenced by a high M_s of 37.8 emu g^{-1} and 90.1% degradation of amoxicillin in 2 hours with 20 mM H_2O_2 and 0.5 g L^{-1} TiO_2–GO-18 wt% Fe_3O_4.[129] Apart from semiconductors, MOF is also a proper choice to combine

Table 3 Application of MRNPCs in photocatalytic Fenton-like processes

MNPC	Method of synthesis	Target pollutant	Working conditions							Ref.
			Pollutant dose	Catalyst dose	H_2O_2 dose	Light source	Time (min)	M_s (emu g^{-1})	Removal efficiency	
Fe_3O_4@rGO@AgI	Co-precipitation	Phenol	50 mg L^{-1}	0.57 g L^{-1}	0.2 mM	UV-C	540	N/A	93%	126
Fe_3O_4@MIL-100(Fe)	Microwave-assisted *in situ* synthesis	Diclofenac	60 mg L^{-1}	0.1 g L^{-1}	40 mM	VIS	180	15.1	>99%	127
Fe_3O_4–GO	Co-precipitation and hydrothermal method	Phenol	20 mg L^{-1}	0.25 g L^{-1}	10 mM	UV	120	37.9	98.8%	128
TiO_2–GO–Fe_3O_4	Hydrothermal method	Amoxicillin	20 mg L^{-1}	0.5 g L^{-1}	20 mM	VIS	120	37.8	90.1%	129
Yolk–shell $ZnFe_2O_4$	Hydrothermal method	Tetracycline	60 mg L^{-1}	0.3 g L^{-1}	40 mM	VIS	40	N/A	83.8%	130
rGO–$ZnFe_2O_4$	Hydrothermal method	Ciprofloxacin	10 mg L^{-1}	0.3 g L^{-1}	20 mM	Solar light	60	N/A	99%	131
$MnFe_2O_4$/bio-char	Co-precipitation	Tetracycline	40 mg L^{-1}	0.5 g L^{-1}	100 mM	VIS	120	11.75	93%	132
$MnFe_2O_4$/CeO_2/SnS_2	Hydrothermal method	Methylene blue	—	—	—	—	120	N/A	78.8%	133
F-doped g-C_3N_4 coupled $NiFe_2O_4$	Thermal decomposition and sol–gel method	Paracetamol	25 mg L^{-1}	1 g L^{-1}	200 mM	VIS	60	11.05	95%	134
$NiFe_2O_4$–carbon nanotubes	Hydrothermal method	Sulfamethoxazole	5 mg L^{-1}	0.025 g L^{-1}	55 mM	VIS, UV	120	33.1	$P_{[VIS]}$ = ~90% $P_{[UV]}$ = 100%	135
MnFe-LDO-biochar	Co-precipitation	Metronidazole	20 mg L^{-1}	0.4 g L^{-1}	6 mM	UV	300	28.5	98%	136
Fe_3O_4@SiO_2/d-TiO_2/Pt	Co-precipitation	Carbamazepine	14 mg L^{-1}	0.5 g L^{-1}	1.375 mM	UV	120	N/A	~98%	137
Fe_3O_4@S doped-ZnO	Hydrothermal method	Ofloxacin	10 mg L^{-1}	0.25 g L^{-1}	50 mM	Natural light	120	N/A	99.4%	138

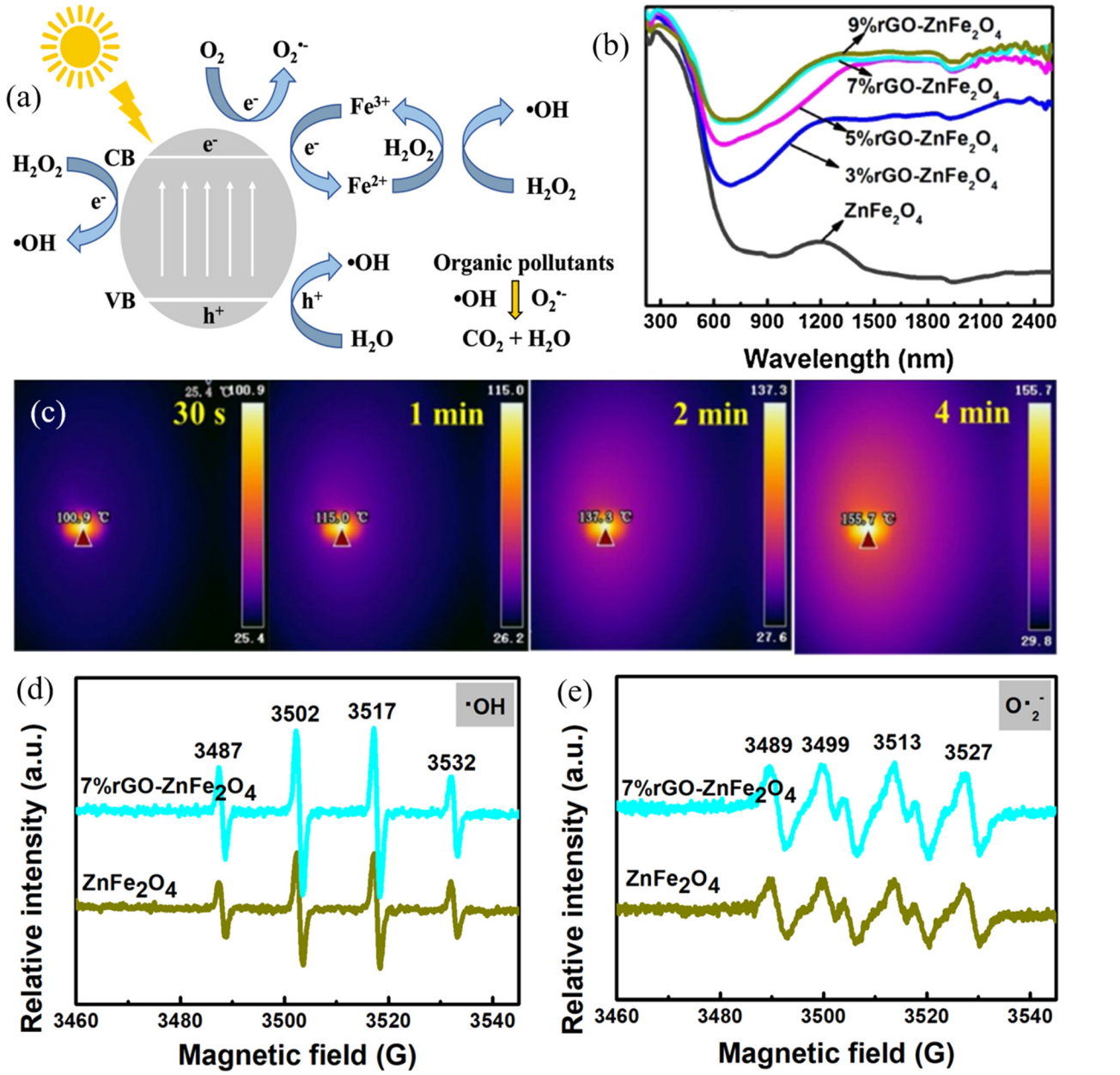

Fig. 5 (a) Schematic diagram showing the mechanism of photocatalytic-Fenton like process using MRNPCs; (b) light adsorption spectra of different rGO-$ZnFe_2O_4$ samples; (c) infrared thermal image of 7% rGO-$ZnFe_2O_4$ under solar light illumination; generation of (d) $^{\bullet}OH$ and (e) $O_2^{\bullet-}$ by $ZnFe_2O_4$ and 7% rGO-$ZnFe_2O_4$ in the photocatalytic-Fenton like processes. Reproduced from ref. 131 with permission from Elsevier, copyright 2021.

with Fe_3O_4 as it can offer external Fe ions for H_2O_2 activation. As an example, Fe_3O_4@MIL-100(Fe) MRNPC was fabricated through an *in situ* microwave method, which showed a remarkably high specific surface area of 1244.6 $m^2\ g^{-1}$. As a result, 60 mg L^{-1} diclofenac (DCF) was completely removed within 2.5 hours under visible light illumination. The excellent performance was caused by the abundant Fe(II)/Fe(III) reactive sites offered by the large surface area and enhanced photocatalytic activity of the material.[127]

Spinel ferrites have been widely investigated as MRNPCs in photocatalytic Fenton-like processes due to their narrow bandgap for utilizing a wide range of solar spectrum and resulting in sufficient generation of charge carriers. $ZnFe_2O_4$ is one of the popular spinel ferrites in photocatalytic Fenton-like processes because it has good chemical stabilities for restraining the leaching of Fe ions under a wide range of circumstances. In light of this, Xiang *et al.* developed the yolk-shell $ZnFe_2O_4$, which can harvest more light within the absorption range and offer a larger surface area compared with the spherical one. As a result, 95.3% of tetracycline and 82.2% of CIP were removed with the addition of 20 mM H_2O_2 in 90 min of

visible light irradiation.[130] Furthermore, the same group hybridized the yolk-shell $ZnFe_2O_4$ with rGO to form a rGO-$ZnFe_2O_4$ nanocomposite. Notably, the incorporation of rGO expanded the light response to the infrared region that enabled rGO-$ZnFe_2O_4$ with photo-thermal conversion (Fig. 5b and c), thereby reducing the activation barrier for H_2O_2 and promoting the generation of $^{\bullet}OH$ and $O_2^{\bullet-}$ (Fig. 5d and e). Subsequently, the time for the complete degradation of CIP was shortened to 40 min.[131]

Spinel ferrites with dual transition metals, such as $MnFe_2O_4$ and $NiFe_2O_4$, are considered as suitable activators of H_2O_2 because they can provide double reactive centers. For example, the $MnFe_2O_4$ synthesized by the sol–gel method can degrade around 94% CIP from DI water in 2 hours under UV-vis irradiation with the addition of H_2O_2, and the material can also work in real wastewater for CIP removal.[142] Additionally, $MnFe_2O_4$/biochar and $MnFe_2O_4/CeO_2/SnS_2$ were also fabricated for organic pollutant removal using the photocatalytic Fenton-like processes.[132,133] Mechanistic investigations in these two studies revealed that both Fe^{2+}/Fe^{3+} and Mn^{2+}/Mn^{3+} pairs and photogenerated electrons participate in H_2O_2 activation, thereby accelerating pollutant degradation. Similarly, the $NiFe_2O_4$-based MRNPCs, mainly $NiFe_2O_4$/carbon nanotubes and $NiFe_2O_4$/F-doped-g-C_3N_4, were also synthesized for organic pollutant removal with the addition of H_2O_2 and achieved excellent performance, primarily owing to the sufficient surface active sites and enhanced photocatalytic activity by carbon material functionalization.[134,135]

Several drawbacks associated with photocatalytic Fenton-like processes using MRNPCs are: (i) the efficacy of the processes is still subject to variations in the pH levels because $^{\bullet}OH$ has less oxidation potential for pollutant degradation in alkaline conditions (E_g = 1.8 eV at pH ≥ 10);[143] (ii) the demand for H_2O_2 increases at neutral pH due to its self-decomposition, thus consuming more H_2O_2 to achieve the same degradation efficiency;[144,145] (iii) MRNPCs are less efficient in wastewater for activating H_2O_2 for pollutant degradation due to the complex wastewater components that can mask active sites of MRNPCs and quench the photogenerated charge carriers; and (iv) material corrosion may occur in some scenario as the iron ions in MRNPCs engage in H_2O_2 activation.

The countermeasures for the above-mentioned drawbacks are: (i) controlling the pH value between 4–10 during the process to avoid the metal leaching and reduction in performance; (ii) using chelating agents like nitrilotriacetic acid and Oxalate $C_2O_4^{2-}$, to form a Fe^{2+} complex at neutral pH, promoting the $^{\bullet}OH$ production;[146] (iii) choosing porous and layered support with high surface areas for the improvement of reaction activity between Fe and H_2O_2;[147] and (iv) the material development should consider the stability of MRNPCs and avoid the use of any toxic material.

4.2 Photocatalytic-assisted sulfate-radicals-based (SR) AOPs

Conventional photocatalysis and most photocatalytic-assisted AOPs produce $^{\bullet}OH$ as the dominant reactive species for pollutant degradation but many components in sewage can quench $^{\bullet}OH$ to restrict their performance.[148] The photocatalytic-assisted SR-AOPs using MRNPCs are less affected by components in water due to the high selectivity of sulfate radicals ($SO_4^{\bullet-}$) towards organic pollutants. The $SO_4^{\bullet-}$ exhibits a greater oxidation potential (E_0 = 2.5–3.1 V) compared to $^{\bullet}OH$ (E_0 = 1.8–2.7 V) and can be generated over a broad pH range ($4 < pH < 9$).[149] The production of $SO_4^{\bullet-}$ through the photocatalytic activation of PDS) or PMS requires less energy consumption compared to other techniques such as electrolysis, ultrasound, and UV irradiation.[150] The PDS/PMS dosages required in photocatalytic SR-AOP using MRNPCs are much lower than that of H_2O_2 in photocatalytic Fenton-like processes because PDS/PMS do not suffer self-decomposition. Moreover, it is safer to store PDS/PMS on a large scale under room temperature and atmospheric pressure compared with H_2O_2.[151] A summary of pertinent details regarding recently reported MRNPCs for the photocatalytic SR-AOPs is presented in Table 4 for comparison.

The mechanism of photocatalytic SR-based AOPs using MRNPCs is shown in Fig. 6a. After light excitation and the production of electrons and holes, they transfer to the material surface and react with PDS/PMS to generate $SO_4^{\bullet-}$ (eqn (9)–(12)).[156] Following this, $SO_4^{\bullet-}$ interacts with H_2O or OH^-, generating $^{\bullet}OH$ (eqn (13)). Transition metals in MRNPCs with lower valence states, such as Fe^{2+}, Cu^{2+}, Ce^{4+}, Ni^{2+}, and Co^{2+}, can effectively activate PDS/PMS. The transition metal M^{n+} can activate PDS/PMS by losing electrons to become $M^{(n+1)+}$, generating $SO_4^{\bullet-}$ or $^{\bullet}OH$ (eqn (14)–(16)).[160] The $M^{(n+1)+}$ can be subsequently reduced to M^{n+} by photogenerated electrons (eqn (17)).

$$S_2O_8^{2-} + e^- \rightarrow SO_4^{2-} + SO_4^{\bullet-} \quad (9)$$

$$HSO_5^- + e^- \rightarrow SO_4^{\bullet-} + OH^- \quad (10)$$

$$HSO_5^- + h^+ \rightarrow SO_5^{\bullet-} + H^+ \quad (11)$$

$$2SO_5^{\bullet-} \rightarrow 2SO_4^{\bullet-} + O_2 \quad (12)$$

$$SO_4^{\bullet-} + H_2O \rightarrow SO_4^{2-} + {}^{\bullet}OH \quad (13)$$

$$M^{n+} + S_2O_8^{2-} \rightarrow M^{(n+1)+} + SO_4^{\bullet-} + SO_4^{2-} \quad (14)$$

$$M^{n+} + HSO_5^- \rightarrow M^{(n+1)+} + SO_4^{\bullet-} + OH^- \quad (15)$$

$$M^{n+} + HSO_5^- \rightarrow M^{(n+1)+} + SO_4^{2-} + {}^{\bullet}OH \quad (16)$$

$$M^{(n+1)+} + e^- \rightarrow M^{n+} \quad (17)$$

In general, the transition metal ions, mainly Fe in MRNPCs, play an important role in activating PDS/PMS and the

Table 4 Application of MRNPCs in photocatalytic sulfate radical based AOPs

MNPC	Method of synthesis	Target pollutant	Working conditions						M_s (emu g^{-1})	Removal efficiency	Ref.
			Pollutant dose	Catalyst dose	Chemical type	Chemical dosage	Light source	Time (min)			
$ZnFe_2O_4$	Sol–gel method	Levofloxacin	10 mg L^{-1}	1 g L^{-1}	PMS	1 mM	LED	180	N/A	88.5%	152
$CuFe_2O_4$/g-C_3N_4	Sol–gel method	Propranolol	0.02 Mol	1 g L^{-1}	PDS	1 mM	VIS	120	22.04	82.2%	36
Fe_3O_4@CeO_2@BiOI	Hydrothermal method	Sulfamethoxazole	0.05 mM	0.1 g L^{-1}	PMS	0.2 mM	UVA	15	N/A	97%	153
MNPs@C	Co-precipitation	Acetaminophen	20 mg L^{-1}	0.16 g L^{-1}	PMS	0.77 mM	UV-C	40	6.3	97%	154
TiO_2/Fe_3O_4/activated carbon	Co-precipitation	Tetracycline	30 mg L^{-1}	0.3 g L^{-1}	PS	3.0 mM	UV-C	60	25.3	96%	155
BiOCl@Fe_3O_4	Co-precipitation	Atenolol	2.5 mg L^{-1}	0.1 g L^{-1}	PMS	0.1 mM	Solar light	60	N/A	70.2%	156
$ZnFe_2O_4$/A-MoS_2	Hydrothermal method	Carbamazepine	2 mg L^{-1}	0.2 g L^{-1}	PMS	0.5 mM	VIS	3	13.5	100%	157
Ti^{3+}–TiO_2/Ar–Fe_2O_3	Hydrothermal method	Norfloxacin	20 mg L^{-1}	0.1 g L^{-1}	PDS	1.5 mM	VIS	30	12.03	98.9%	158
ZnO@SiO_2@Fe_3O_4	Hydrothermal method	Malathion	20 mg L^{-1}	0.3 g L^{-1}	PMS	2 mM	UV	120	35.1	91.2%	159

photogenerated electrons further promote the activation process by accelerating the Fe(II)/Fe(III) cycle. For example, Zhong *et al.* applied $ZnFe_2O_4$ to activate PMS for levofloxacin (LEV) removal under LED illumination, achieving a high degradation efficiency of 88.5% in 3 h. The mechanism studies confirmed the engagement of Fe^{2+}/Fe^{3+} in PMS activation and the photogenerated electrons and holes favored the production of reactive species. Subsequently, $^1O_2$ was found as the dominant reactive species in the $ZnFe_2O_4$/PMS/LED system, in which the $^1O_2$ was generated from $O_2^{\bullet-}$ conversion and PMS activation.[152] Similarly, many other MRNPCs, such as BiOCl@Fe_3O_4, ZnO@SiO_2@Fe_3O_4, and Ti^{3+}–TiO_2/Ar–Fe_2O_3, also activated PDS/PMS using Fe^{2+}/Fe^{3+} pairs and photogenerated charge carriers, leading to highly efficient pollutant removal.

The integration of a magnetic material with a transition metal-based photocatalyst to form MRNPC is an appropriate strategy to further enhance the performance of photocatalytic-assisted SR-AOP as it introduces more reactive sites to the MRNPC. For instance, Zheng *et al.* developed an S-scheme $ZnFe_2O_4$/A-MoS_2 heterojunction to activate PMS for carbamazepine degradation, achieving excellent performance with 100% removal in 3 minutes. The density functional theory calculation revealed that the photogenerated electrons transferred to the $ZnFe_2O_4$ reactive center for PMS activation (Fig. 6b). As shown in Fig. 6c and d, XPS spectra confirmed that both Fe and Mo engaged in PMS activation and Fe made a dominant contribution. Overall, this study highlighted the important roles of photogenerated electron and reactive sites (Fe and Mo) in the efficient activation of PMS (Fig. 6e).[157] Likewise, Fe_3O_4@CeO_2@BiOI nanospheres were fabricated for PMS activation to degrade sulfamethoxazole. An extremely high performance of 97% SMX degradation was obtained within 15 minutes under UVA irradiation with a low PMS dosage of 0.2 mM PMS. The excellent performance was ascribed to the material providing Fe^{2+}/Fe^{3+} and Ce^{4+}/Ce^{3+} dual reactive centers and generating abundant charge carriers for PMS activation.[153]

On the other hand, activation of PMS using the magnetic heterojunction $SrTiO_3/BaFe_{12}O_{19}$ for the tetracycline degradation in wastewater has been proved to not involve the state transformation of metallic elements of Sr, Ti, Ba and Fe, as consistent binding energies of these elements before and after reaction are observed. Improved efficiency on the tetracycline degradation using heterostructure $SrTiO_3/BaFe_{12}O_{19}$ is attributed to the enhanced adsorption of PMS on the composite than on $SrTiO_3$, as well as the more effective electron migration inside the composite.[161] Moreover, Yan *et al.* observed the role of Ba in reinforcing the stability of metal elements in the heterojunction composites. It supports the point that enhancement of efficiency of photocatalysis-assisted PMS reaction derives from the boosted electron utility.[162]

In additions, many researchers have combined carbon-based materials, such as g-C_3N_4, activated carbon, carbon sphere, and MOF, in the MRNPCs because such materials can regulate the charge transfer for enhanced PDS/PMS activation. For example, the visible-light responsive $CuFe_2O_4$/g-C_3N_4 MRNPC was developed for PDS activation and achieved an 82.2% removal of propranolol in 2 hours with 1 mM PDS. Mechanistic investigations revealed that PDS acted as a photogenerated electron acceptor from g-C_3N_4 to generate $SO_4^{\bullet-}$, while the self-redox cycles of Fe and Cu further facilitated PDS activation.[36] Likewise, Noorisepehr *et al.* applied Fe_3O_4/activated carbon (MNPs@C) to activate PMS for acetaminophen oxidation, resulting in a high degradation efficiency of 97% in 40 min under UV light. The study found that activated carbon was a promoter of PMS activation, which can directly decompose PMS to produce $SO_4^{\bullet-}$ and improve the charge transfer ability of the material to enhance PMS activation using charge carriers.[154] In

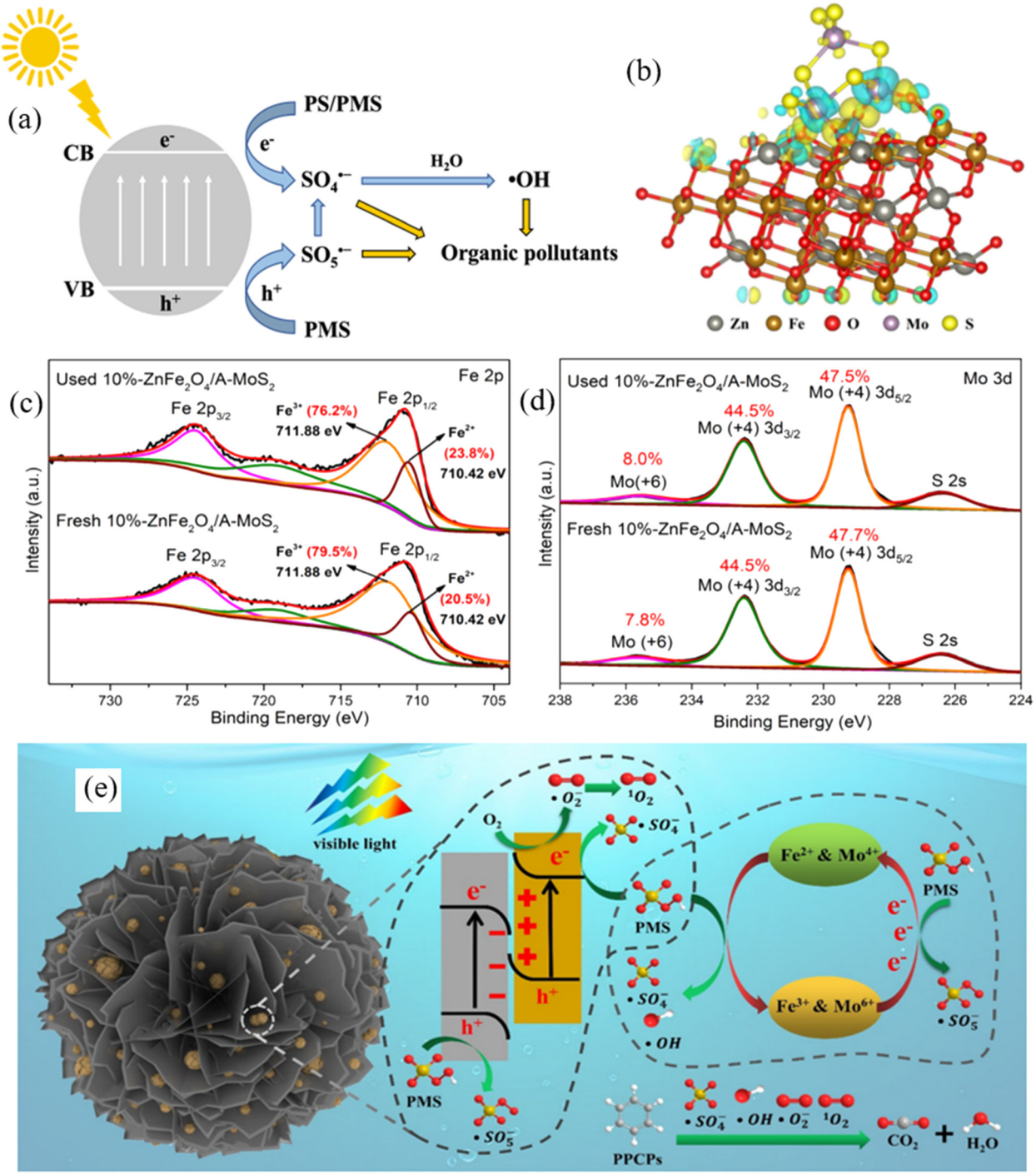

Fig. 6 (a) Mechanism of photocatalytic SR-based AOPs using MRNPCs; (b) charge density difference shows the charge transfer from A-MoS_2 to $ZnFe_2O_4$ in the $ZnFe_2O_4$/A-MoS_2 S-scheme heterojunction; XPS spectra of (c) Fe 2p and (d) Mo 3p in 10%-$ZnFe_2O_4$/A-MoS_2 before and after use; (e) mechanism of PPCP removal in the PC/PMS system using 10%-$ZnFe_2O_4$/A-MoS_2. Reproduced from ref. 157 with permission from American Chemical Society, copyright 2023.

addition, TiO_2/Fe_3O_4/activated carbon (TFOC) was applied for PDS activation to degrade tetracycline, showing a high removal efficiency of 96% in 60 min. The study found that surface functional groups in activated carbon, such as –COOH and C═O, interacted with PDS molecules to facilitate $SO_4^{\bullet-}$ generation.[155]

Nevertheless, several limitations of photocatalytic SR-AOPs using MRNPCs should be noted. (i) The remaining PDS/PMS in water brings additive toxicity that may pose negative effects on ecosystems and human health.[163] Additionally, sulfate, the end product of PDS/PMS decomposition, is expected to have a high concentration in water after

treatment that requires further treatment. (ii) The transition metals may leach into the solution and enter the environment after several cycles of treatment. The leaching of transition metals is mainly ascribed to the acidic solution where transition metals have a higher solubility and the material corrosion caused by $SO_4^{\bullet-}$.[164] (iii) Contaminants and PDS/PMS may potentially compete for active sites, which ultimately determines the degradation performance and reaction rate. However, distinguishing between active sites for contaminant degradation and persulfate activation remains a challenge.[165]

Possible countermeasures are needed for the above-mentioned issues. (i) Novel MRNPCs with high efficiency in activating low dosages of PDS/PMS are urgently needed, thereby minimizing PDS/PMS residues and reducing negative effects from sulfate generation. (ii) Researchers are encouraged to choose environmentally friendly catalyst materials containing unharmful metals, with modifications to prevent leaching. (iii) More in-depth mechanisms can be explored by employing density functional theory calculations.

4.3 Photocatalytic ozonation

Photocatalytic ozonation combines the merits of photocatalysis and ozone activation to promote the generation of reactive oxygen species for efficient mineralization of organic pollutants. Such a configuration can solve the high charge recombination of conventional photocatalysis because ozone can react with electrons to facilitate charge separation. Ozone is a powerful oxidant agent (E_0 = 2.80 eV) that can quickly react with the photogenerated electrons at the catalyst surface to form the $^{\bullet}OH$, thereby enhancing the separation of e^-/h^+.[166] The combined method named photocatalytic ozonation has a higher mineralization rate compared to conventional photocatalysis and ozonation due to the above-mentioned synergistic effects.[167] As a result, this process also reduces the toxicity from the intermediates of pollutant degradation. Table 5 summarizes the pertinent details of representative MRNPCs employed in photocatalytic ozonation.

In photocatalytic ozonation using MRNPCs, $^{\bullet}OH$ is the dominant reactive species for pollutant degradation that can be produced *via* ozone activation in three pathways (Fig. 7a). First, ozone can be activated by UV light and further form $^{\bullet}OH$ through the reaction with water (eqn (18) and (19)).[177] Second, ozone reacts with water to generate H_2O_2, which can be cleaved into $^{\bullet}OH$ by UV light (eqn (20) and (21)).[178] Second, ozone can be reduced by electrons to ozonide radicals (eqn (22)), which further react with H^+ to produce $^{\bullet}OH$ (eqn (23) and (24)).[179] Third, the $O_2^{\bullet-}$ produced through the reaction between oxygen and electrons (eqn (3)) can also react with ozone to generate ozonide radicals (eqn (25)) and further produce $^{\bullet}OH$ through a chain reaction (eqn (23) and (24)).[178]

$$O_3 + h\nu \rightarrow O^{\bullet} + O_2 \quad (18)$$

$$O^{\bullet} + H_2O \rightarrow 2^{\bullet}OH \quad (19)$$

$$O_3 + H_2O + UV \rightarrow H_2O_2 + O_2 \quad (20)$$

$$H_2O_2 + UV \rightarrow 2^{\bullet}OH \quad (21)$$

$$O_3 + e^- \rightarrow O_3^{\bullet-} \quad (22)$$

$$O_3^{\bullet-} + H^+ \rightarrow HO_3^{\bullet} \quad (23)$$

$$HO_3^{\bullet} \rightarrow {}^{\bullet}OH + O_2 \quad (24)$$

$$O_2^{\bullet-} + O_3 \rightarrow O_3^{\bullet-} + O_2 \quad (25)$$

The light sources significantly affect the yielding amount of hydroxyl radicals. At an early stage, researchers applied the energy-intensive UV light to excite MRNPCs in photocatalytic ozonation, resulting in high production of hydroxyl radicals. For example, Mahmoodi *et al.* employed a nickel–zinc ferrite as MRNPC to activate ozone for dye degradation under UV light, achieving complete decolorization of the dye in 28 minutes under optimal conditions. The study found that $^{\bullet}OH$ played a dominant role in dye removal and UV light played an important role in $^{\bullet}OH$ generation.[168]

To save treatment costs, solar light was applied as the light source for photocatalytic ozonation using MRNPCs. A TiO_2-coated magnetic activated carbon (TiFeC) was synthesized *via* the sol–gel method, achieving complete pollutant degradation and high TOC removal (90%) using photocatalytic ozonation. The study compared TOC removal under irradiation at different wavelength ranges, mainly 300–800, 320–800, and 390–800 nm, and found that the UV light in the solar spectrum significantly improved the mineralization of the contaminant.[169] Likewise, a magnetic 3-D structure g-C_3N_4/Fe-MCM-48 was prepared to activate ozone for azithromycin degradation. The introduction of Fe-MCM-48 increased the surface areas from 5.3 $m^2\ g^{-1}$ to 165 $m^2\ g^{-1}$, enhanced the mass transfer capabilities, and broadened the light absorption edge from 457 nm to 545 nm (Fig. 7b). The presence of Fe also accelerated O_3 activation and significantly reduced charge recombination (Fig. 7c), eventually enhancing the production of photogenerated electrons for ozone activation. As a result, 98.8% of azithromycin was removed in 11 min under simulated solar light (Fig. 7d). Fig. 7e shows the overall mechanisms of the photocatalytic ozonation using g-C_3N_4/Fe-MCM-48. The developed g-C_3N_4/Fe-MCM-48 achieved enhanced O_3 activation due to the improved separation of photogenerated electrons, increased Fe active sites, and enlarged surface area, thereby facilitating the production of reactive species for enhanced azithromycin degradation.[170]

In the case of using visible light, hydroxyl radicals are only generated *via* ozone activation over photogenerated charge carriers. Moreover, the selection and modification of different MRNPCs are affected by the light sources used, and the narrow band gap spinel ferrites are desirable choices in

Table 5 Application of MRNPCs in the photocatalytic ozonation processes

MNPC	Method of synthesis	Target pollutant	Working conditions						M_s (emu g^{-1})	Removal efficiency	Ref.
			Pollutant dose	Catalyst dose	Gas flow rate	Ozone concn.	Light source	Time (min)			
Nickel–zinc ferrite	Hydrothermal method	Dye	150 mg L^{-1}	0.005 g L^{-1}	0.08 L min^{-1}	55 g m^{-3}	UV	28	56	100%	168
TiO_2–magnetic carbon (TiFeC)	Sol–gel method	Metoprolol tartrate	50 mg L^{-1}	0.25 g L^{-1}	20 L h^{-1}	6 mg L^{-1}	Solar light	120	4.4	98%	169
g-C_3N_4/Fe-MCM-48	Hydrothermal method	Azithromycin	50 mg L^{-1}	4 g L^{-1}	1 L min^{-1}	50 mg L^{-1}	Solar light	11	0.25	98.8%	170
$ZnFe_2O_4$@carbon	Hydrothermal method	Oxalic acid	260 mg L^{-1}	2 g L^{-1}	40 mL min^{-1}	10 mg L^{-1}	VIS	60	N/A	$P_{[Toc]}$ = 87%	171
$BiFeO_3$	Thermal decomposition	Norfloxacin	10 mg L^{-1}	0.2 g L^{-1}	75 mg h^{-1}	N/A	VIS	60	1.75	83.3%	172
TiO_2/Fe_3O_4/C	Sol–gel method	Metoprolol tartrate	2 mg L^{-1}	0.4 g L^{-1}	20 L h^{-1}	10 mg L^{-1}	Solar light	30	4.2	100%	173
Fe_3O_4@TiO_2	Sol–gel method	Dipyrone	0.3 mM	1 g L^{-1}	30 L h^{-1}	10 mg L^{-1}	UV	180	N/A	60%	174
N-TiO_2/$ZnFe_2O_4$/zeolite	Sol–gel method	Cephalexin	100 mg L^{-1}	2 g L^{-1}	500 mg h^{-1}	N/A	VIS	120	N/A	95%	175
g-C_3N_4/$FeVO_2$/Fe@NH_2-biochar	Hydrothermal method	Methyl paraben	20 mg L^{-1}	0.5 g L^{-1}	N/A	4.8 mg L^{-1}	Solar light	60	30	99.8%	176

this scenario. For instance, the $ZnFe_2O_4$@carbon (ZFO@C) was fabricated using a one-pot hydrothermal method, in which the carbon layer provided good conductivity and acted like an ozone activator resulting in 87% removal of TOC in oxalic acid degradation in 1 h under visible light. The band gap for the ZFO@C was about 1.82 eV, lower than the pristine $ZnFe_2O_4$.[171] Moreover, magnetic $BiFeO_3$ nanoparticles with a narrow band gap of 2.14 eV were also applied for oxalic acid decontamination using photocatalytic ozonation, achieving an 83.3% removal rate after 1 hour of reaction under visible light.[172]

Several limitations associated with photocatalytic ozonation using MRNPCs are summarized. (i) Photocatalytic ozonation is still considered to be one of the costlier treatment technologies. (ii) The performance of photocatalytic ozonation is significantly affected by the dosages of ozone, pollutant concentrations, and other substances in water.[180] (iii) Certain reaction intermediates, such as particular carboxylic acids, are hardly eliminated by ozone or its resulting oxidizing radicals, and can pose a potential environmental hazard.[181]

Possible solutions for the above-mentioned challenges are proposed. (i) Considering the economic effect, photocatalytic ozonation should only be used against the recalcitrant contaminants after the primary treatment. (ii) To achieve better performance, it is crucial to ensure the good dissolution of ozone molecules in the aqueous solution and proper pretreatment should be conducted to remove the water components that negatively affect photocatalytic ozonation. (iii) In order to guarantee the safety of intermediates, it is recommended that both TOC removal efficiency and toxicity testing be carried out.

4.4 Sono-photocatalytic process

The sono-photocatalytic process involves the use of a combination of ultraviolet radiation, ultrasonic sound waves, and a photocatalyst to produce reactive species for pollutant removal. It has been developed to prevent MRNPC aggregation and refresh the MRNPC surface for improved performance in organic pollutant degradation. As for the mechanism, MRNPC absorbs light to produce charge carriers for radicals generation and ultrasound creates cavitation bubbles to generate highly reactive species. Thus, more reactive species can be utilized for pollutant degradation compared to conventional photocatalysis. Accordingly, Kakavandi *et al.* impregnated TiO_2 on magnetic activated carbon for TC degradation subjected to ultrasonic and ultraviolet irradiation. Single treatments of ultrasonic irradiation (2.1%) or photocatalysis (44.9%) were found to be ineffective, while the sono-photocatalytic process resulted in removal efficiencies of 93%. The study found that the employment of ultrasound suppressed the recombination of charge carriers and stimulated the oxidation reaction, thus achieving a synergistic effect. Moreover, heat energy was generated during the reaction, which in turn excites the MRNPC, forming additional free radicals.[38]

However, sono-photocatalysis suffers two drawbacks, mainly that the degradation efficiency is pH-dependent, and additional electrical energy is required.[182,183] Due to high energy consumption, this technology lacks detailed investigation and still requires further development. Recently, other than applying energy-intensive ultrasonics, pictures of harvesting natural mechanical energies, such as waving and water flow vibration and wind, have attracted wide attention. The piezo effect of ferroelectric materials makes the combination of sono-photocatalysis possibly practical. Natural mechanical energies are available by sono-reaction under all types of weather regardless of solar irradiation conditions, whereas photocatalysis harvests solar energy. It allows the 24 hour continuous function of the sono-photocatalysis reaction-driven green and natural energies.[184]

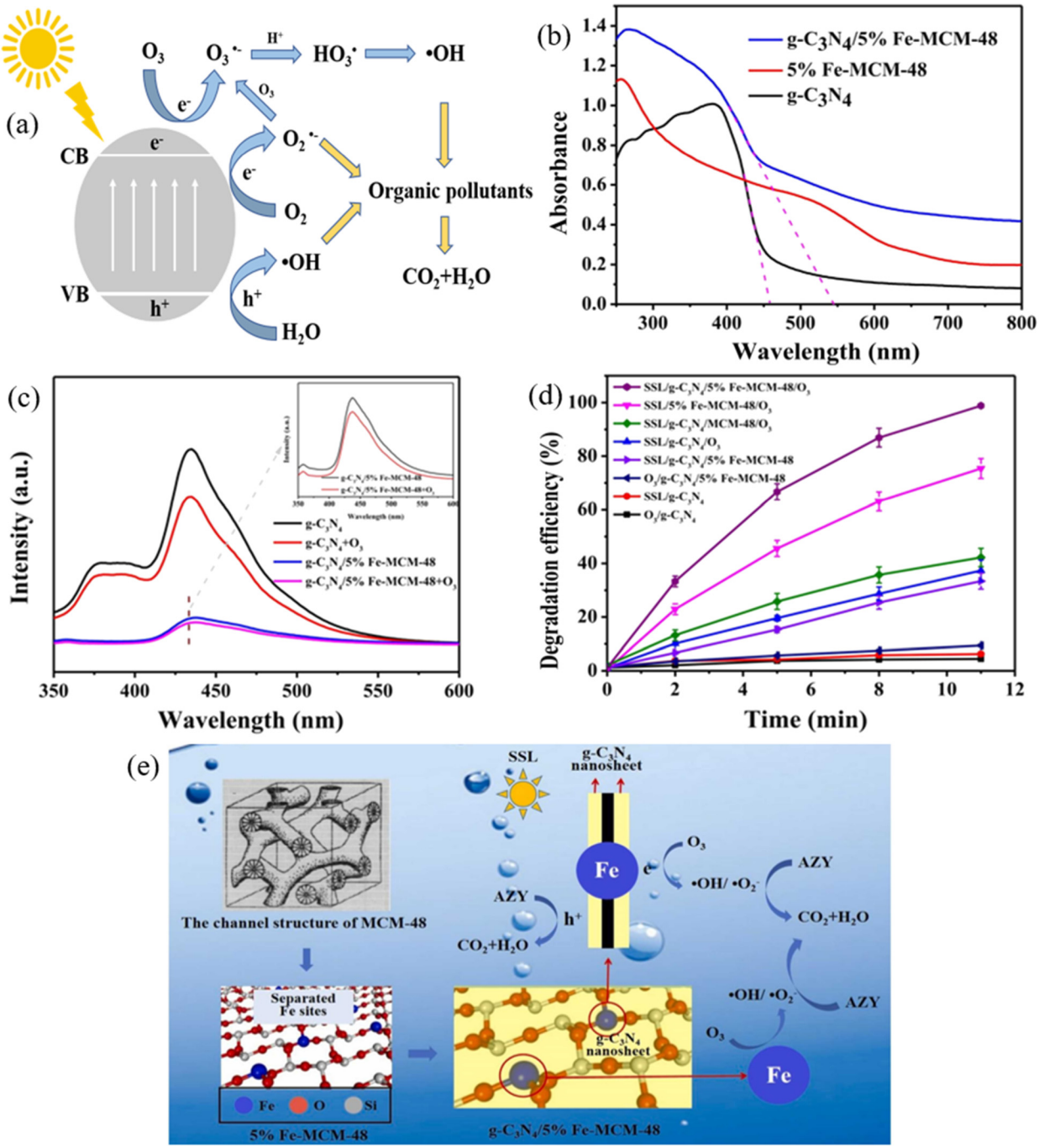

Fig. 7 (a) Schematic diagram showing the mechanisms of photocatalytic ozonation using MRNPCs; (b) N_2 adsorption–desorption isotherms, (c) light adsorption ability, and (d) PL spectra of g-C_3N_4, 5% Fe-MCM-48, and g-C_3N_4/5% Fe-MCM-48; (e) proposed mechanisns of azithromycin degradation by photocatalytic ozonation using g-C_3N_4/5% Fe-MCM-48. Reproduced from ref. 170 with permission from Elsevier, copyright 2023.

5. Challenges and perspectives for practical applications of MRNPCs

The practical application of MRNPCs in real environmental conditions is still challenging. Several important issues regarding material development, recycling, stability, environmental effectiveness, and reactor designs for MRNPC applications remain (Fig. 8a) and should be properly addressed.

5.1 Material development

Material development is fundamental in the practical application of MRNPCs, where the main challenges that

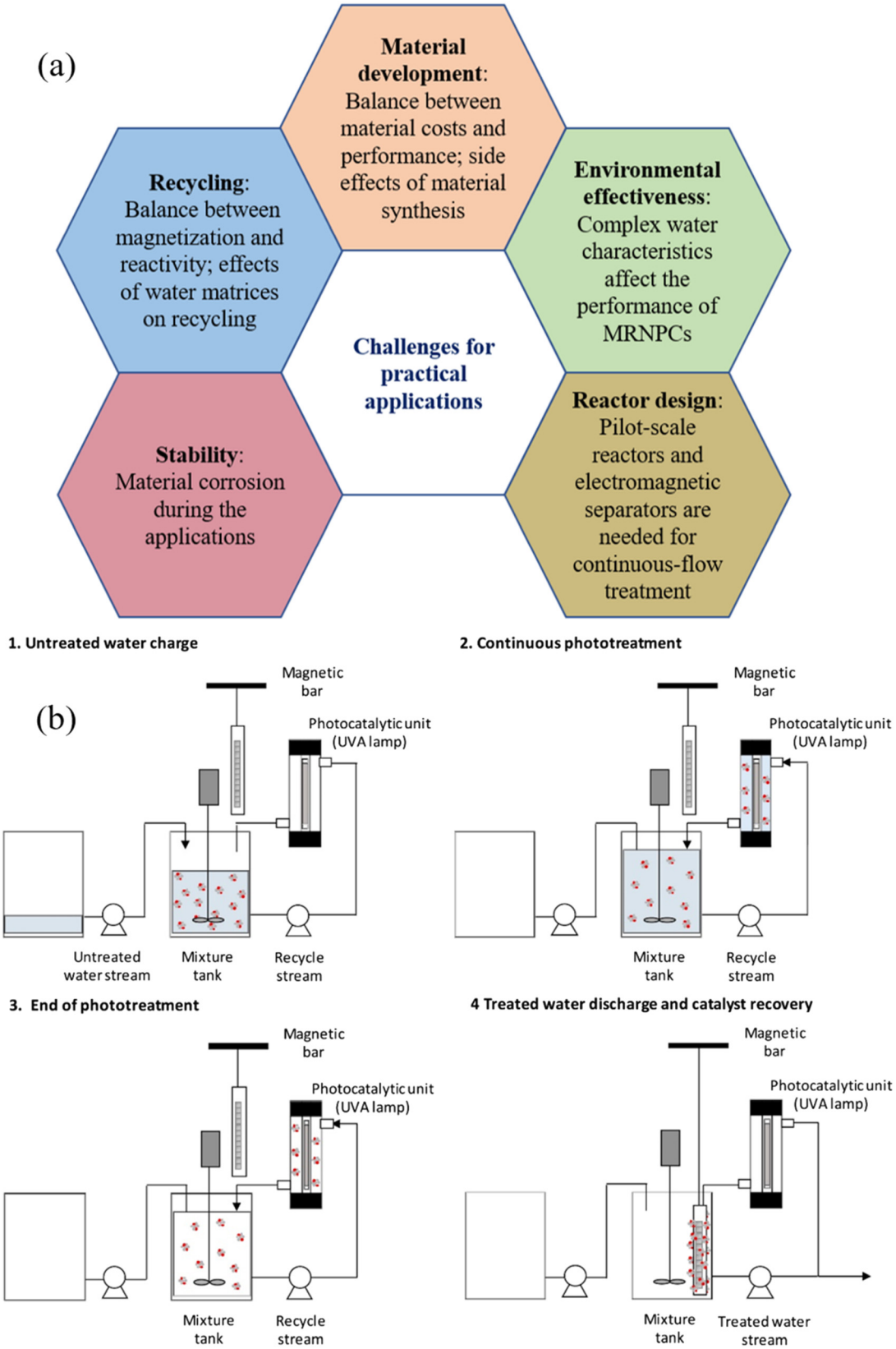

Fig. 8 (a) Challenges of MNRPCs in practical applications; (b) operation of magnetic photocatalytic reactor: 1) loading of MNRPCs and water, 2) continuous phototreatment; 3) end of phototreatment, 4) MNRPCs recycling. Reproduced from ref. 70 with permission from Elsevier, copyright 2019.

come from this aspect are how to balance the material costs and performance and how to reduce the side effects caused by material synthesis. The properties of the MRNPCs, mainly particle sizes and shapes, band gap, chemical composition, and magnetic behavior, play critical roles in determining the efficiency of the catalytic reaction. As reviewed above, MRNPCs composed of a pristine photocatalyst and a magnetic material are cost-effective but less efficient due to their intrinsic poor properties. Consequently, various modifications are employed to vary the characteristics of MRNPCs for better performance. However, such modifications involve complex synthesis approaches or the use of noble materials, which significantly increase the cost of MRNPC development. Taking elemental doping as an example, non-metal doping requires high temperatures and complicated pathways that result in high cost, while doping with noble metal ions, like Ag, is effective in improving material performance but costly. Moreover, doping transition elements allows MRNPCs posse spin polarization which provides spin electron freedom to enhance magnetic property, benefiting the collection and recycling of particularly the 2D structural photocatalysts.[185] In light of this, researchers are suggested to reduce the material cost by adopting cost-effective components in MRNPC modifications and developing novel approaches with mild reaction conditions and simple operation for material fabrication.

Side effects brought by MRNPC synthesis are generally ignored by researchers in scientific reports. Most importantly, some MRNPC fabrication approaches, mainly thermal decomposition and sol–gel method, involve the use of hazardous chemical solvents, which may pose health risks to the experimentalists. The waste solutions containing hazardous chemicals also need to be carefully treated to avoid any environmental pollution and safety issues. Furthermore, many synthesis approaches, such as thermal decomposition, hydrothermal synthesis, and microemulsion method, are energy-intensive due to the requirement of high temperatures, pressure, or long reaction duration. Consequently, these methods are regarded as high carbon emission types that restrain the decarbonization progress. Additionally, some fabrication methods suffer low MRNPC yield, even at high chemical dosages, leading to serious chemical waste, potential secondary pollution, and high expenses. To overcome the above challenges, green synthesis is encouraged to be used in MRNPC production because (i) it employs green chemicals with a high material yield, thereby avoiding chemical waste; and (ii) it consumes less energy during the synthesis process through producing materials in ambient conditions.

5.2 Recycling

Recycling MRNPCs from the treated water is critical for its practical application. The main challenge of MRNPCs regarding their recycling is to ensure an appropriate saturation magnetization intensity of the materials while maintaining a high photocatalytic reactivity. Generally, magnetic separation is possible if the M_s of MRNPC is at least 1.0 emu g^{-1}.[186] The M_s of the reviewed MRNPCs ranged from 0.25 to 56 emu g^{-1}. The vast majority of MRNPCs have a M_s above the minimum requirement and can be separated within a few minutes. The magnetic properties of the employed magnetic materials are determined by its crystal structure. He *et al.* reported that the γ-Fe_2O_3 resulting from the calcination of Fe_3O_4 particles possesses a much lower M_s value than that of Fe_3O_4.[83] In addition, the M_s of an MRNPC is also affected by the ratio of magnetic material. For instance, Wang *et al.* compared the saturation magnetism values of MRNPCs containing different proportions of Fe_3O_4 and found that 5%-Fe_3O_4/GE/SCN has a lower magnetization than 20%-Fe_3O_4/GE/SCN.[80] Therefore, more attention should be given to maintaining high magnetization of magnetic material during synthesis and adjusting a rational ratio between the magnetic material and photocatalyst in MRNPCs to balance the materials' performance and recycling function.

Apart from the MRNPCs themselves, the water matrices and the developed electromagnetic separator can also affect the magnetic recycling of the materials. Ahmed *et al.* applied the Fe_3O_4/$La(OH)_3$ composite in a pilot scale reactor for real river water treatment and found that the recycling efficiency of the material decreased with operation time with an average recovery efficiency of 44.34%, which was much lower than that of the batch test in the lab using a simple magnet (>98%).[187] The major reason for the phenomenon was the complex components in the target water, mainly organic matters and suspended solids, affected the separation of Fe_3O_4/$La(OH)_3$ from the treated water by being adsorbed by the material to reduce the magnetic property or block the transfer of the magnetic material toward separator. On the other hand, the poor capacity of the developed electromagnetic drum in collecting Fe_3O_4/$La(OH)_3$ from the treated water in a continuous flow also decreased the separation efficiency of Fe_3O_4/$La(OH)_3$. Therefore, the applied MRNPCs for target water with complex components should possess an extremely high magnetic property against interference from the water matrices. Additionally, developing an efficient electromagnetic separator on a large scale for the separation of MRNPCs is also necessary for stepping the related techniques forward in industrial wastewater treatment.

5.3 Stability

Apart from recycling, the stability of MRNPCs plays an important role in practical application as good stability can ensure long-term operation in reality. During the application, MRNPCs face the challenge of material corrosion that adversely affects long-term usage, causes performance loss, and may bring secondary pollution. The corrosion is mainly caused by redox reactions, especially in photocatalytic Fenton-like processes and photocatalytic-assisted SR-AOPs where the Fe iron participates in the activation of oxidants.

Most researchers mainly focus on the performance of the developed MRNPCs but do not pay enough attention to the potential material corrosion. Therefore, researchers should seek strategies to enhance the stability of MRNPCs against corrosion. For example, Feng *et al.* and Yan *et al.* introduced Ba in iron oxide magnetic core to enhance photocatalytic activity and simultaneously prevent metal ion leaching.[161,162] Moreover, the potential stability loss of MRNPCs during photocatalytic applications should be monitored by comparing the used MRNPCs and the fresh ones in terms of chemical composition, crystal structure, morphology, photocatalytic and photoelectrochemical properties. For example, XPS, XRD, and Fourier-transform infrared (FT-IR) spectra can be used to measure the variations in chemical compositions, crystalline structure, and functional groups, respectively.[104,107,114,173] The morphology and microstructure of the recycled catalyst are demonstrated using SEM and TEM.[188,189] By comprehensively characterizing the MRNPCs before and after use, the mechanisms of material corrosion can be revealed. Researchers should further analyze the obtained data to find out appropriate approaches to avoid the material corrosion of MRNPCs in the photocatalysis or photocatalysis-involving processes or regenerate the material after a certain duration of use, thereby ensuring long-term operation and reducing performance loss.

5.4 Environmental effectiveness

In practical applications, the characteristics of wastewater are also key factors influencing the performance of MRNPCs. Most of the reviewed studies investigated the performance of MRNPCs under ideal conditions using solutions consisting only of deionized (DI) water and one single contaminant, which can not reflect reality. For example, Kumar *et al.* found that the IBU degradation efficiency using g-C_3N_4/TiO_2/Fe_3O_4@SiO_2 significantly dropped from 98% in DI water to 13% in secondary treated sewage, indicating sewage components negatively affected the performance of MRNPCs.[103] In general, anions, natural organic matter (NOM), and suspended solids are the main components in wastewater that restrain organic pollutant removal. Several ions, mainly SO_4^{2-}, $H_2PO_4^-$, Cl^-, and HCO_3^-, can scavenge $^{\bullet}OH$ and other reactive species to reduce the oxidation capacity of MRNPCs.[188] Moreover, NO_3^- and $H_2PO_4^-$ are also found to occupy the surface reactive sites of MRNPCs due to their strong affinity toward MRNPCs, thereby interfering with the interaction between the contaminant and material, reducing degradation efficiency.[190] NOM affects the performance of MRNPCs mainly in three pathways by competing with organic pollutants for reactive species, adsorbing solar light in 200–700 nm to decrease the light absorption of MRNPCs, and being adsorbed by MRNPCs to mask the reactive sites.[190] Likewise, suspended solids also restrict pollutant degradation by blocking MRNPCs' light absorption. Therefore, it is recommended that the MRNPCs should be developed with real wastewater as the target to ensure the practicability of the materials. Moreover, researchers are encouraged to fabricate MRNPCs that are more adaptable over a wide range of environmental conditions for organic pollutant degradation. On the other hand, for treating wastewater with complicated compositions, pretreatments are necessary to minimize the potential negative influence.

5.5 Reactor design

Reactor design is essential for scaling up the application of MRNPCs from laboratory investigation to the industrial level. In most reviewed studies, most pollutant degradation using MRNPCs was conducted in simple batch reactors with a limited volume of hundreds of mL and external magnetic materials were used to separate the MRNPCs, which is impractical in water treatment plants. More efforts should be made to develop S with magnetic separators integrated for practical operation. For example, Fernández *et al.* have made progress towards practical application by fabricating a sequential batch reactor equipped with an internal magnetic separator that can be used for treating wastewater with a continuous flow. As shown in Fig. 8b, an electromagnetic separator was employed to allow the easy separation of MRNPC from the treated water for reuse. Moreover, the sequential batch reactor achieved better performance in antibiotic removal than the bench-scale photoreactor, mainly due to the better dispersion of the catalyst.[70] However, the developed reactor was limited to lab-scale operation using synthetic wastewater, and the pilot-scale reactors with real wastewater as the target are still pending investigation.

Furthermore, the high-gradient magnetic separator has been one of the most common magnetic filters used for magnetic separation on a large scale. By adding a ferromagnetic matrix of fine wires or rods into the magnetic field, the magnetic solids are captured on the matrix for separation.[191] However, there are concerns regarding this separator as undesired non-magnetic entrainment may occur during the separation process, leading to a deterioration in the quality of the separated magnetic materials. With the development of the separator, many methods for improving separation selectivity have been incorporated into industrial applications, and researchers need to select a suitable separator based on the characteristics of the MRNPCs. Moreover, characteristics of the target water such as turbidity, suspended solids, and organic matter should be considered when designing a separator intended for use at the pilot scale. Additionally, several factors about the application scenario should be fully considered for the separator design, such as the size of the reactor, the amount of material collected, and the effects of water flow.

6. Conclusions

Over the past decade, due to the beauties of MRNPCs over conventional photocatalysts in easy recycling and high reactivity, MRNPCs have been widely investigated and applied in either conventional photocatalysis or photocatalysis-

assisted processes for efficient organic pollutant removal. In conventional photocatalysis, several modifications, mainly element doping, heterojunction formation, and hybrid functionalization, have been verified as effective strategies to improve material performance due to the increased charge carrier production and restrained recombination. As for photocatalysis-assisted processes, both photogenerated charge carriers and transition metal ions in MRNPCs engaged in the activation of oxidants, increasing the production of reactive species to accelerate organic pollutant degradation. Nevertheless, several challenges of MRNPCs toward practical applications, in terms of material development, recycling, stability, and reactor, design are pointed out. Perspectives about these issues are also provided accordingly: (i) cost-effective chemicals are recommended in MRNPC production to reduce material costs and green synthesis is encouraged to avoid the side effects raised by MRNPC synthesis; (ii) the fabrication of MRNPCs should consider the balance between performance and recycling to ensure the magnetic separation of MRNPCs from real wastewater; (iii) multiple approaches should be employed to comprehensively evaluate the stability of MRNPCs in long-term operation; (iv) MRNPCs with wide adaptability and pretreatment are encouraged to reduce the interference from environmental effectiveness; and (v) continuous flow reactors equipped with suitable magnetic separators should be developed. Hence, specific experiments should be designed against the challenges of MRNPCs in practical applications for organic pollutant removal. Moreover, pilot-scale studies using real contaminated water as the target are also encouraged to step forward the related techniques to the industrial level.

Conflicts of interest

The authors declare that they have no known competing financial interests or personal relationships that could have appeared to influence the work reported in this paper.

Acknowledgements

The authors gratefully acknowledge the Research Grants Council of Hong Kong for providing financial support for this research under the General Research Fund (16202220).

References

1 M. B. Ahmed, J. L. Zhou, H. H. Ngo, W. Guo, N. S. Thomaidis and J. Xu, Progress in the biological and chemical treatment technologies for emerging contaminant removal from wastewater: a critical review, *J. Hazard. Mater.*, 2017, **323**, 274–298.

2 A. R. Khataee and M. B. Kasiri, Photocatalytic degradation of organic dyes in the presence of nanostructured titanium dioxide: Influence of the chemical structure of dyes, *J. Mol. Catal. A: Chem.*, 2010, **328**, 8–26, DOI: **10.1016/j.molcata.2010.05.023**.

3 P. Singh, K. Sharma, V. Hasija, V. Sharma, S. Sharma, P. Raizada, M. Singh, A. K. Saini, A. Hosseini-Bandegharaei and V. K. Thakur, Systematic review on applicability of magnetic iron oxides–integrated photocatalysts for degradation of organic pollutants in water, *Mater. Today Chem.*, 2019, **14**, 100186, DOI: **10.1016/j.mtchem.2019.08.005**.

4 S. Uhlenbrook and R. Connor, *The United Nations world water development report 2019: leaving no one behind*. 2019.

5 A. Pattnaik, J. N. Sahu, A. K. Poonia and P. Ghosh, Current perspective of nano-engineered metal oxide based photocatalysts in advanced oxidation processes for degradation of organic pollutants in wastewater, *Chem. Eng. Res. Des.*, 2023, **190**, 667–686, DOI: **10.1016/j.cherd.2023.01.014**.

6 H. K. Paumo, S. Dalhatou, L. M. Katata-Seru, B. P. Kamdem, J. O. Tijani, V. Vishwanathan, A. Kane and I. Bahadur, TiO_2 assisted photocatalysts for degradation of emerging organic pollutants in water and wastewater, *J. Mol. Liq.*, 2021, **331**, 115458, DOI: **10.1016/j.molliq.2021.115458**.

7 N. Agasti, V. Gautam, Priyanka, Manju, N. Pandey, M. Genwa, P. Meena, S. Tandon and R. Samantaray, Carbon nanotube based magnetic composites for decontamination of organic chemical pollutants in water: A review, *Appl. Surf. Sci. Adv.*, 2022, **10**, 100270, DOI: **10.1016/j.apsadv.2022.100270**.

8 M. J. Jacinto, L. F. Ferreira and V. C. Silva, Magnetic materials for photocatalytic applications—a review, *J. Sol-Gel Sci. Technol.*, 2020, **96**, 1–14.

9 N. Chaukura, E. S. Muzawazi, G. Katengeza and A. E. D. Mahmoud, Chapter 20 - Remediation technologies for contaminated soil systems, in: *Emerging Contaminants in the Terrestrial-Aquatic-Atmosphere Continuum*, ed. W. Gwenzi, Elsevier, 2022, pp. 353–365.

10 A. J. Ebele, M. Abou-Elwafa Abdallah and S. Harrad, Pharmaceuticals and personal care products PPCPs in the freshwater aquatic environment, *Emerging Contam.*, 2017, **3**, 1–16, DOI: **10.1016/j.emcon.2016.12.004**.

11 V. Hasija, P. Raizada, A. Sudhaik, P. Singh, V. K. Thakur and A. A. P. Khan, Fabrication of $Ag/AgI/WO_3$ heterojunction anchored P and S co-doped graphitic carbon nitride as a dual Z scheme photocatalyst for efficient dye degradation, *Solid State Sci.*, 2020, **100**, 106095, DOI: **10.1016/j.solidstatesciences.2019.106095**.

12 N. Chandel, K. Sharma, A. Sudhaik, P. Raizada, A. Hosseini-Bandegharaei, V. K. Thakur and P. Singh, Magnetically separable $ZnO/ZnFe_2O_4$ and $ZnO/CoFe_2O_4$ photocatalysts supported onto nitrogen doped graphene for photocatalytic degradation of toxic dyes, *Arabian J. Chem.*, 2020, **13**, 4324–4340, DOI: **10.1016/j.arabjc.2019.08.005**.

13 X. Zhu and D. Jassby, Electroactive membranes for water treatment: Enhanced treatment functionalities, energy considerations, and future challenges, *Acc. Chem. Res.*, 2019, **52**, 1177–1186.

14 P. Singh, B. Priya, P. Shandilya, P. Raizada, N. Singh, B. Pare and S. B. Jonnalagadda, Photocatalytic mineralization

of antibiotics using 60%WO_3/BiOCl stacked to graphene sand composite and chitosan, *Arabian J. Chem.*, 2019, **12**, 4627–4645, DOI: **10.1016/j.arabjc.2016.08.005**.

15 L. Xu, J. Xia, H. Xu, S. Yin, K. Wang, L. Huang, L. Wang and H. Li, Reactable ionic liquid assisted solvothermal synthesis of graphite-like C_3N_4 hybridized α-Fe_2O_3 hollow microspheres with enhanced supercapacitive performance, *J. Power Sources*, 2014, **245**, 866–874, DOI: **10.1016/j.jpowsour.2013.07.014**.

16 W. S. Chai, J. Y. Cheun, P. S. Kumar, M. Mubashir, Z. Majeed, F. Banat, S. H. Ho and P. L. Show, A review on conventional and novel materials towards heavy metal adsorption in wastewater treatment application, *J. Cleaner Prod.*, 2021, **296**, 126589.

17 J. He, J. Cheng and I. M. Lo, Green photocatalytic disinfection of real sewage: efficiency evaluation and toxicity assessment of eco-friendly TiO2-based magnetic photocatalyst under solar light, *Water Res.*, 2021, **190**, 116705.

18 A. Kumar, P. Raizada, P. Singh, R. V. Saini, A. K. Saini and A. Hosseini-Bandegharaei, Perspective and status of polymeric graphitic carbon nitride based Z-scheme photocatalytic systems for sustainable photocatalytic water purification, *Chem. Eng. J.*, 2020, **391**, 123496, DOI: **10.1016/j.cej.2019.123496**.

19 M. Li, Y. Liu, G. Zeng, N. Liu and S. Liu, Graphene and graphene-based nanocomposites used for antibiotics removal in water treatment: A review, *Chemosphere*, 2019, **226**, 360–380, DOI: **10.1016/j.chemosphere.2019.03.117**.

20 H. Do, L. Phan Thi, N. H. Dao Nguyen, C. Huang, Q. V. Le and V. Nguyen, Tailoring photocatalysts and elucidating mechanisms of photocatalytic degradation of perfluorocarboxylic acids PFCAs in water: a comparative overview, *J. Chem. Technol. Biotechnol.*, 2020, **95**, 2569–2578.

21 D. Zhu and Q. Zhou, Action and mechanism of semiconductor photocatalysis on degradation of organic pollutants in water treatment: A review, *Environ. Nanotechnol., Monit. Manage.*, 2019, **12**, 100255, DOI: **10.1016/j.enmm.2019.100255**.

22 M. Yang, G. Ma, H. Yang, Z. Xiaoqiang, W. Yang and H. Hou, Advanced strategies for promoting the photocatalytic performance of $FeVO_4$ based photocatalysts: A review of recent progress, *J. Alloys Compd.*, 2023, **941**, 168995, DOI: **10.1016/j.jallcom.2023.168995**.

23 N. P. Radhika, R. Selvin, R. Kakkar and A. Umar, Recent advances in nano-photocatalysts for organic synthesis, *Arabian J. Chem.*, 2019, **12**, 4550–4578, DOI: **10.1016/j.arabjc.2016.07.007**.

24 T. Naseem and T. Durrani, The role of some important metal oxide nanoparticles for wastewater and antibacterial applications: A review, *Environ. Chem. Ecotoxicol.*, 2021, **3**, 59–75, DOI: **10.1016/j.enceco.2020.12.001**.

25 E. Roduner, Size matters: why nanomaterials are different, *Chem. Soc. Rev.*, 2006, **35**, 583–592.

26 J. Hu, C. Sun, L. Wu, G. Zhao, H. Liu and F. Jiao, Halogen doped g-C_3N_4/ZnAl-LDH hybrid as a Z-scheme photocatalyst for efficient degradation for tetracycline in seawater, *Sep. Purif. Technol.*, 2023, **309**, 123047.

27 S. K. Fanourakis, J. Peña-Bahamonde, P. C. Bandara and D. F. Rodrigues, Nano-based adsorbent and photocatalyst use for pharmaceutical contaminant removal during indirect potable water reuse, *npj Clean Water*, 2020, **3**, 1.

28 C. McCullagh, N. Skillen, M. Adams and P. K. Robertson, Photocatalytic reactors for environmental remediation: a review, *J. Chem. Technol. Biotechnol.*, 2011, **86**, 1002–1017.

29 M. A. Lazar, S. Varghese and S. S. Nair, Photocatalytic water treatment by titanium dioxide: recent updates, *Catalysts*, 2012, **2**, 572–601.

30 N. Ahmadpour, M. H. Sayadi, S. Sobhani and M. Hajiani, Photocatalytic degradation of model pharmaceutical pollutant by novel magnetic TiO_2@$ZnFe_2O_4$/Pd nanocomposite with enhanced photocatalytic activity and stability under solar light irradiation, *J. Environ. Manage.*, 2020, **271**, 110964.

31 N. Nasseh, T. J. Al-Musawi, M. R. Miri, S. Rodriguez-Couto and A. H. Panahi, A comprehensive study on the application of $FeNi_3$@SiO_2@ZnO magnetic nanocomposites as a novel photo-catalyst for degradation of tamoxifen in the presence of simulated sunlight, *Environ. Pollut.*, 2020, **261**, 114127.

32 Y. R. Yao, W. Z. Huang, H. Zhou, Y. F. Zheng and X. C. Song, Self-assembly of dandelion-like Fe_3O_4@C@BiOCl magnetic nanocomposites with excellent solar-driven photocatalytic properties, *J. Nanopart. Res.*, 2014, **16**, 1–9.

33 S. H. S. Chan, T. Yeong Wu, J. C. Juan and C. Y. Teh, Recent developments of metal oxide semiconductors as photocatalysts in advanced oxidation processes AOPs for treatment of dye waste-water, *J. Chem. Technol. Biotechnol.*, 2011, **86**, 1130–1158.

34 J. Li, M. Zhang, X. Li, Q. Li and J. Yang, Effect of the calcination temperature on the visible light photocatalytic activity of direct contact Z-scheme g-C_3N_4-TiO_2 heterojunction, *Appl. Catal., B*, 2017, **212**, 106–114.

35 L. Yang, Y. Xiang, F. Jia, L. Xia, C. Gao, X. Wu, L. Peng, J. Liu and S. Song, Photo-thermal synergy for boosting photo-Fenton activity with rGO-$ZnFe_2O_4$: Novel photo-activation process and mechanism toward environment remediation, *Appl. Catal., B*, 2021, **292**, 120198, DOI: **10.1016/j.apcatb.2021.120198**.

36 R. Li, M. Cai, Z. Xie, Q. Zhang, Y. Zeng, H. Liu, G. Liu and W. Lv, Construction of heterostructured $CuFe_2O_4$/g-C_3N_4 nanocomposite as an efficient visible light photocatalyst with peroxydisulfate for the organic oxidation, *Appl. Catal., B*, 2019, **244**, 974–982, DOI: **10.1016/j.apcatb.2018.12.043**.

37 A. Rey, D. H. Quiñones, P. M. Álvarez, F. J. Beltrán and P. K. Plucinski, Simulated solar-light assisted photocatalytic ozonation of metoprolol over titania-coated magnetic activated carbon, *Appl. Catal., B*, 2012, **111–112**, 246–253, DOI: **10.1016/j.apcatb.2011.10.005**.

38 B. Kakavandi, N. Bahari, R. Rezaei Kalantary and E. Dehghani Fard, Enhanced sono-photocatalysis of tetracycline antibiotic using TiO_2 decorated on magnetic

activated carbon MAC@T coupled with US and UV: A new hybrid system, *Ultrason. Sonochem.*, 2019, **55**, 75–85, DOI: **10.1016/j.ultsonch.2019.02.026**.

39 S. Nizamuddin, M. Siddiqui, N. M. Mubarak, H. A. Baloch, E. C. Abdullah, S. A. Mazari, G. J. Griffin, M. P. Srinivasan and A. Tanksale, Iron oxide nanomaterials for the removal of heavy metals and dyes from wastewater, *Nanoscale Mater. Water Purif.*, 2019, 447–472.

40 M. M. S. Sanad, M. M. Farahat, S. I. El-Hout and S. M. El-Sheikh, Preparation and characterization of magnetic photocatalyst from the banded iron formation for effective photodegradation of methylene blue under UV and visible illumination, *J. Environ. Chem. Eng.*, 2021, **9**, 105127, DOI: **10.1016/j.jece.2021.105127**.

41 G. K. Rozenberg, L. S. Dubrovinsky, M. P. Pasternak, O. Naaman, T. Le Bihan and R. Ahuja, High-pressure structural studies of hematite Fe_2O_3, *Phys. Rev. B: Condens. Matter Mater. Phys.*, 2002, **65**, 064112.

42 C. Santhosh, A. Malathi, E. Dhaneshvar, A. Bhatnagar, A. N. Grace and J. Madhavan, Iron oxide nanomaterials for water purification, in: *Nanoscale materials in water purification*, Elsevier, 2019, pp. 431–446.

43 K. Zhang, Y. Liu, J. Deng, S. Xie, H. Lin, X. Zhao, J. Yang, Z. Han and H. Dai, Fe_2O_3/3DOM $BiVO_4$: High-performance photocatalysts for the visible light-driven degradation of 4-nitrophenol, *Appl. Catal., B*, 2017, **202**, 569–579.

44 U. T. Lam, R. Mammucari, K. Suzuki and N. R. Foster, Processing of iron oxide nanoparticles by supercritical fluids, *Ind. Eng. Chem. Res.*, 2008, **47**, 599–614.

45 S. Thomas, D. Pasquini, S. Leu and D. A. Gopakumar, Chapter 20 - Magnetic Nanoparticles for Water Purification, in: *Nanoscale Materials in Water Purification*, ed. S. Thomas, D. Pasquini, S. Leu and D.A. Gopakumar, Elsevier, 2019, pp. 521–552.

46 W. Wu, Z. Wu, T. Yu, C. Jiang and W. Kim, Recent progress on magnetic iron oxide nanoparticles: synthesis, surface functional strategies and biomedical applications, *Sci. Technol. Adv. Mater.*, 2015, **16**, 023501.

47 M. Nirouei, A. Jafari and K. Boustani, Magnetic and structural study of $FeNi_3$ nanoparticles: effect of calcination temperature, *J. Supercond. Novel Magn.*, 2014, **27**, 2803–2811.

48 C. Xue, Q. Zhang, J. Li, X. Chou, W. Zhang, H. Ye, Z. Cui and P. J. Dobson, Noninvasively modifying band structures of wide-bandgap metal oxides to boost photocatalytic activity, *J. Nanomater.*, 2013, **2013**, 2.

49 T. Sugimoto and E. Matijević, Formation of uniform spherical magnetite particles by crystallization from ferrous hydroxide gels, *J. Colloid Interface Sci.*, 1980, **74**, 227–243.

50 T. K. Indira and P. K. Lakshmi, Magnetic nanoparticles–a review, *Int. J. Pharm. Sci. Nanotechnol.*, 2010, **3**, 1035–1042.

51 X. Li, G. Xu, Y. Liu and T. He, Magnetic Fe_3O_4 nanoparticles: Synthesis and application in water treatment, *Nanosci. Nanotechnol.–Asia*, 2011, **1**, 14–24.

52 S. Shylesh, V. Schünemann and W. R. Thiel, Magnetically separable nanocatalysts: bridges between homogeneous and heterogeneous catalysis, *Angew. Chem., Int. Ed.*, 2010, **49**, 3428–3459.

53 A. Lu, E. E. Salabas and F. Schüth, Magnetic nanoparticles: synthesis, protection, functionalization, and application, *Angew. Chem., Int. Ed.*, 2007, **46**, 1222–1244.

54 S. D. Roy, K. C. Das and S. S. Dhar, Conventional to green synthesis of magnetic iron oxide nanoparticles; its application as catalyst, photocatalyst and toxicity: A short review, *Inorg. Chem. Commun.*, 2021, **134**, 109050, DOI: **10.1016/j.inoche.2021.109050**.

55 C. Li, Y. Wei, A. Liivat, Y. Zhu and J. Zhu, Microwave-solvothermal synthesis of Fe_3O_4 magnetic nanoparticles, *Mater. Lett.*, 2013, **107**, 23–26.

56 A. Lu, E. E. Salabas and F. Schüth, Magnetic nanoparticles: synthesis, protection, functionalization, and application, *Angew. Chem., Int. Ed.*, 2007, **46**, 1222–1244.

57 F. Sharifianjazi, M. Moradi, N. Parvin, A. Nemati, A. Jafari Rad, N. Sheysi, A. Abouchenari, A. Mohammadi, S. Karbasi, Z. Ahmadi, A. Esmaeilkhanian, M. Irani, A. Pakseresht, S. Sahmani and M. Shahedi Asl, Magnetic $CoFe_2O_4$ nanoparticles doped with metal ions: A review, *Ceram. Int.*, 2020, **46**, 18391–18412, DOI: **10.1016/j.ceramint.2020.04.202**.

58 I. Fatimah, G. Fadillah and S. P. Yudha, Synthesis of iron-based magnetic nanocomposites: a review, *Arabian J. Chem.*, 2021, **14**, 103301.

59 K. K. Kefeni, T. A. Msagati and B. B. Mamba, Ferrite nanoparticles: synthesis, characterisation and applications in electronic device, *Mater. Sci. Eng., B*, 2017, **215**, 37–55.

60 N. H. Nam and N. H. Luong, Nanoparticles: Synthesis and applications, in: *Materials for biomedical engineering*, Elsevier, 2019, pp. 211–240.

61 H. Itoh and T. Sugimoto, Systematic control of size, shape, structure, and magnetic properties of uniform magnetite and maghemite particles, *J. Colloid Interface Sci.*, 2003, **265**, 283–295.

62 Z. Chen, C. Wu, Z. Zhang, W. Wu, X. Wang and Z. Yu, Synthesis, functionalization, and nanomedical applications of functional magnetic nanoparticles, *Chin. Chem. Lett.*, 2018, **29**, 1601–1608.

63 N. Chavan, D. Dharmaraj, S. Sarap and C. Surve, Magnetic nanoparticles – A new era in nanotechnology, *J. Drug Delivery Sci. Technol.*, 2022, **77**, 103899, DOI: **10.1016/j.jddst.2022.103899**.

64 A. Mirzaei, L. Yerushalmi, Z. Chen, F. Haghighat and J. Guo, Enhanced photocatalytic degradation of sulfamethoxazole by zinc oxide photocatalyst in the presence of fluoride ions: Optimization of parameters and toxicological evaluation, *Water Res.*, 2018, **132**, 241–251.

65 J. Hu, G. Zhao, L. Wu, C. Sun, X. Long, X. Long and F. Jiao, Designing and Fabricating a Vulcanized ZnAl LDH-Modified g-C3N4 Heterojunction for Enhanced Visible-Light-Driven Photocatalytic Degradation Activity, *Ind. Eng. Chem. Res.*, 2022, **61**, 15225–15239.

66 C. Sun, L. Wu, J. Hu, S. A. Hussain, J. Yang and F. Jiao, A novel dual S-scheme heterojunction photocatalyst β-Bi_2O_3/

NiAl-LDH/α-Bi_2O_3 induced by phase-transformed bismuth oxide for efficient degradation of antibiotics in full-spectrum: Degradation pathway, DFT calculation and mechanism insight, *Chem. Eng. J.*, 2023, **474**, 145616.

67 H. De Lasa and B. Serrano-Rosales, *Advances in chemical engineering: photocatalytic technologies*, Academic Press, 2009.

68 J. Chang, Q. Zhang, Y. Liu, Y. Shi and Z. Qin, Preparation of Fe_3O_4/TiO_2 magnetic photocatalyst for photocatalytic degradation of phenol, *J. Mater. Sci.: Mater. Electron.*, 2018, **29**, 8258–8266.

69 E. Mrotek, S. Dudziak, I. Malinowska, D. Pelczarski, Z. Ryżyńska and A. Zielińska-Jurek, Improved degradation of etodolac in the presence of core–shell $ZnFe_2O_4/SiO_2/TiO_2$ magnetic photocatalyst, *Sci. Total Environ.*, 2020, **724**, 138167, DOI: **10.1016/j.scitotenv.2020.138167**.

70 L. Fernández, M. Gamallo, M. A. González-Gómez, C. Vázquez-Vázquez, J. Rivas, M. Pintado and M. T. Moreira, Insight into antibiotics removal: Exploring the photocatalytic performance of a Fe_3O_4/ZnO nanocomposite in a novel magnetic sequential batch reactor, *J. Environ. Manage.*, 2019, **237**, 595–608, DOI: **10.1016/j.jenvman.2019.02.089**.

71 A. Mirzaei, Z. Chen, F. Haghighat and L. Yerushalmi, Magnetic fluorinated mesoporous g-C_3N_4 for photocatalytic degradation of amoxicillin: Transformation mechanism and toxicity assessment, *Appl. Catal., B*, 2019, **242**, 337–348, DOI: **10.1016/j.apcatb.2018.10.009**.

72 D. Chen, Y. Cheng, N. Zhou, P. Chen, Y. Wang, K. Li, S. Huo, P. Cheng, P. Peng, R. Zhang, L. Wang, H. Liu, Y. Liu and R. Ruan, Photocatalytic degradation of organic pollutants using TiO_2-based photocatalysts: A review, *J. Cleaner Prod.*, 2020, **268**, 121725, DOI: **10.1016/j.jclepro.2020.121725**.

73 L. Wang, J. Zhao, H. Liu and J. Huang, Design, modification and application of semiconductor photocatalysts, *J. Taiwan Inst. Chem. Eng.*, 2018, **93**, 590–602, DOI: **10.1016/j.jtice.2018.09.004**.

74 Z. Yu, X. Chen, X. Kang, Y. Xie, H. Zhu, S. Wang, S. Ullah, H. Ma, L. Wang and G. Liu, Noninvasively modifying band structures of wide-bandgap metal oxides to boost photocatalytic activity, *Adv. Mater.*, 2018, **30**, 1706259.

75 C. B. Anucha, I. Altin, E. Bacaksiz and V. N. Stathopoulos, Titanium dioxide TiO_2-based photocatalyst materials activity enhancement for contaminants of emerging concern CECs degradation: In the light of modification strategies, *Chem. Eng. J. Adv.*, 2022, **10**, 100262, DOI: **10.1016/j.ceja.2022.100262**.

76 N. Kovalevskiy, D. Selishchev, D. Svintsitskiy, S. Selishcheva, A. Berezin and D. Kozlov, Synergistic effect of polychromatic radiation on visible light activity of N-doped TiO_2 photocatalyst, *Catal. Commun.*, 2020, **134**, 105841.

77 M. Ratova, G. T. West, P. J. Kelly, X. Xia and Y. Gao, Synergistic effect of doping with nitrogen and molybdenum on the photocatalytic properties of thin titania films, *Vacuum*, 2015, **114**, 205–212.

78 F. Hu, W. Luo, C. Liu, H. Dai, X. Xu, Q. Yue, L. Xu, G. Xu, Y. Jian and X. Peng, Fabrication of graphitic carbon nitride functionalized P–$CoFe_2O_4$ for the removal of tetracycline under visible light: Optimization, degradation pathways and mechanism evaluation, *Chemosphere*, 2021, **274**, 129783, DOI: **10.1016/j.chemosphere.2021.129783**.

79 A. Kumar, M. Khan, L. Fang and I. M. C. Lo, Visible-light-driven N-TiO_2@SiO_2@Fe_3O_4 magnetic nanophotocatalysts: Synthesis, characterization, and photocatalytic degradation of PPCPs, *J. Hazard. Mater.*, 2019, **370**, 108–116, DOI: **10.1016/j.jhazmat.2017.07.048**.

80 L. Wang, Q. Sun, Y. Dou, Z. Zhang, T. Yan and Y. Li, Fabricating a novel ternary recyclable Fe_3O_4/graphene/sulfur-doped g-C_3N_4 composite catalyst for enhanced removal of ranitidine under visible-light irradiation and reducing of its N-nitrosodimethylamine formation potential, *J. Hazard. Mater.*, 2021, **413**, 125288, DOI: **10.1016/j.jhazmat.2021.125288**.

81 Z. He, T. Hong, J. Chen and S. Song, A magnetic TiO_2 photocatalyst doped with iodine for organic pollutant degradation, *Sep. Purif. Technol.*, 2012, **96**, 50–57, DOI: **10.1016/j.seppur.2012.05.005**.

82 Q. Jiang, H. Yu, C. Zhao, Z. Han, J. Li, J. Zhang and Z. Cheng, In-situ construction of magnetic raspberry-like ZnO/C supporting different transition metal Fe, Co, Ni species with high adsorption-photocatalysis efficiency, *J. Cleaner Prod.*, 2023, **395**, 136443.

83 M. He, D. Li, D. Jiang and M. Chen, Magnetically separable γ-Fe_2O_3@SiO_2@Ce-doped TiO_2 core–shell nanocomposites: Fabrication and visible-light-driven photocatalytic activity, *J. Solid State Chem.*, 2012, **192**, 139–143, DOI: **10.1016/j.jssc.2012.04.004**.

84 B. Cui, H. Peng, H. Xia, X. Guo and H. Guo, Magnetically recoverable core–shell nanocomposites γ-Fe_2O_3@SiO_2@TiO_2–Ag with enhanced photocatalytic activity and antibacterial activity, *Sep. Purif. Technol.*, 2013, **103**, 251–257, DOI: **10.1016/j.seppur.2012.10.008**.

85 M. I. Khan, A. Suleman, M. S. Hasan, S. S. Ali, T. I. Al-Muhimeed, A. A. AlObaid, M. Iqbal, M. M. Almoneef and N. Alwadai, Effect of Ce doping on the structural, optical, and photovoltaic properties of TiO_2 based dye-sensitized solar cells, *Mater. Chem. Phys.*, 2021, **274**, 125177, DOI: **10.1016/j.matchemphys.2021.125177**.

86 M. Cao, P. Wang, Y. Ao, C. Wang, J. Hou and J. Qian, Visible light activated photocatalytic degradation of tetracycline by a magnetically separable composite photocatalyst: Graphene oxide/magnetite/cerium-doped titania, *J. Colloid Interface Sci.*, 2016, **467**, 129–139, DOI: **10.1016/j.jcis.2016.01.005**.

87 P. Yu, S. S. Wang, H. H. Li and W. X. Li, N, Fe Co-doped TiO_2 photocatalyst preparation by sol-gel method with visible light response, *Adv. Mater. Res.*, 2013, **726**, 673–676.

88 Y. Niu, M. Xing, J. Zhang and B. Tian, Visible light activated sulfur and iron co-doped TiO_2 photocatalyst for the photocatalytic degradation of phenol, *Catal. Today*, 2013, **201**, 159–166.

89 Y. Chen, Q. Wu, N. Bu, J. Wang and Y. Song, Magnetic recyclable lanthanum-nitrogen co-doped titania/strontium ferrite/diatomite heterojunction composite for enhanced visible-light-driven photocatalytic activity and recyclability, *Chem. Eng. J.*, 2019, **373**, 192–202, DOI: **10.1016/j.cej.2019.05.047**.

90 D. Kanakaraju, F. D. anak Kutiang, Y. C. Lim and P. S. Goh, Recent progress of Ag/TiO_2 photocatalyst for wastewater treatment: Doping, co-doping, and green materials functionalization, *Appl. Mater. Today*, 2022, **27**, 101500, DOI: **10.1016/j.apmt.2022.101500**.

91 C. B. Anucha, I. Altin, E. Bacaksız, T. Kucukomeroglu, M. H. Belay and V. N. Stathopoulos, Enhanced photocatalytic activity of $CuWO_4$ doped TiO_2 photocatalyst towards carbamazepine removal under UV irradiation, *Separations*, 2021, **8**, 25.

92 C. B. Anucha, I. Altin, E. Bacaksiz, V. N. Stathopoulos, I. Polat, A. Yasar and Ö F. Yüksel, Silver doped zinc stannate Ag-$ZnSnO_3$ for the photocatalytic degradation of caffeine under UV irradiation, *Water*, 2021, **13**, 1290.

93 J. Low, J. Yu, M. Jaroniec, S. Wageh and A. A. Al-Ghamdi, Heterojunction photocatalysts, *Adv. Mater.*, 2017, **29**, 1601694.

94 S. Demirci, T. Dikici, M. Yurddaskal, S. Gultekin, M. Toparli and E. Celik, Synthesis and characterization of Ag doped TiO_2 heterojunction films and their photocatalytic performances, *Appl. Surf. Sci.*, 2016, **390**, 591–601.

95 W. Zhang, X. Xiao, Y. Li, X. Zeng, L. Zheng and C. Wan, Liquid-exfoliation of layered MoS_2 for enhancing photocatalytic activity of TiO_2/g-C_3N_4 photocatalyst and DFT study, *Appl. Surf. Sci.*, 2016, **389**, 496–506.

96 A. Abdel-Wahab, A. Al-Shirbini, O. Mohamed and O. Nasr, Photocatalytic degradation of paracetamol over magnetic flower-like TiO_2/Fe_2O_3 core–shell nanostructures, *J. Photochem. Photobiol., A*, 2017, **347**, 186–198, DOI: **10.1016/j.jphotochem.2017.07.030**.

97 X. Jiang, M. Wang, B. Luo, Z. Yang, W. Li, D. Zhang, X. Pu and P. Cai, Magnetically recoverable flower-like Sn_3O_4/$SnFe_2O_4$ as a type-II heterojunction photocatalyst for efficient degradation of ciprofloxacin, *J. Alloys Compd.*, 2022, **926**, 166878, DOI: **10.1016/j.jallcom.2022.166878**.

98 S. Sharma, V. Dutta, P. Raizada, A. Singh, P. Singh, T. Ahamad, Q. Van Le and V. Nguyen, Type-II heterojunction-based magnetic $ZnFe_2O_4$@$CuFe_2O_4$@SiO_2 photocatalyst for photodegradation of toxic dyes from wastewater, *Appl. Nanosci.*, 2022, 1–15.

99 X. Li, J. He, W. Zhang, L. You and J. Li, Ag nanoparticles interlayered Fe_3O_4/Ag/m TiO_2-ZrO_2 magnetic photocatalysts with enhanced stability and photocatalytic performance for Cr VI reduction, *Appl. Surf. Sci.*, 2023, **607**, 155076.

100 S. Feizpoor and A. Habibi-Yangjeh, Ternary TiO_2/Fe_3O_4/$CoWO_4$ nanocomposites: Novel magnetic visible-light-driven photocatalysts with substantially enhanced activity through p–n heterojunction, *J. Colloid Interface Sci.*, 2018, **524**, 325–336, DOI: **10.1016/j.jcis.2018.03.069**.

101 A. Habibi-Yangjeh and M. Shekofteh-Gohari, Novel magnetic Fe_3O_4/ZnO/$NiWO_4$ nanocomposites: Enhanced visible-light photocatalytic performance through p–n heterojunctions, *Sep. Purif. Technol.*, 2017, **184**, 334–346, DOI: **10.1016/j.seppur.2017.05.007**.

102 H. Li, W. Tu, Y. Zhou and Z. Zou, Z-Scheme photocatalytic systems for promoting photocatalytic performance: recent progress and future challenges, *Adv. Sci.*, 2016, **3**, 1500389.

103 A. Kumar, M. Khan, J. He and I. M. C. Lo, Visible–light–driven magnetically recyclable terephthalic acid functionalized g–C_3N_4/TiO_2 heterojunction nanophotocatalyst for enhanced degradation of PPCPs, *Appl. Catal., A*, 2020, **270**, 118898, DOI: **10.1016/j.apcatb.2020.118898**.

104 R. Rajendran, S. Vignesh, V. Raj, B. Palanivel, A. M. Ali, M. A. Sayed and M. Shkir, Designing of TiO_2/α-Fe_2O_3 coupled g-C_3N_4 magnetic heterostructure composite for efficient Z-scheme photo-degradation process under visible light exposures, *J. Alloys Compd.*, 2022, **894**, 162498, DOI: **10.1016/j.jallcom.2021.162498**.

105 T. He, Y. Wu, C. Jiang, Z. Chen, Y. Wang, G. Liu, Z. Xu, G. Ning, X. Chen and Y. Zhao, *PLoS One*, 2020, **15**, e0237389.

106 S. Raha and M. Ahmaruzzaman, Facile fabrication of g-C_3N_4 supported Fe3O4 nanoparticles/ZnO nanorods: A superlative visible light responsive architecture for express degradation of pantoprazole, *Chem. Eng. J.*, 2020, **387**, 123766, DOI: **10.1016/j.cej.2019.123766**.

107 N. Zhang, X. Li, Y. Wang, B. Zhu and J. Yang, Fabrication of magnetically recoverable Fe_3O_4/CdS/g-C_3N_4 photocatalysts for effective degradation of ciprofloxacin under visible light, *Ceram. Int.*, 2020, **46**, 20974–20984, DOI: **10.1016/j.ceramint.2020.05.158**.

108 P. Shao, J. Tian, B. Liu, W. Shi, S. Gao, Y. Song, M. Ling and F. Cui, Morphology-tunable ultrafine metal oxide nanostructures uniformly grown on graphene and their applications in the photo-Fenton system, *Nanoscale*, 2015, **7**, 14254–14263.

109 M. Moztahida, J. Jang, M. Nawaz, S. Lim and D. S. Lee, Effect of rGO loading on Fe_3O_4: A visible light assisted catalyst material for carbamazepine degradation, *Sci. Total Environ.*, 2019, **667**, 741–750, DOI: **10.1016/j.scitotenv.2019.02.376**.

110 G. Su, L. Liu, X. Liu, L. Zhang, J. Xue and A. Tang, Magnetic Fe_3O_4@SiO_2@$BiFeO_3$/rGO composite for the enhanced visible-light catalytic degradation activity of organic pollutants, *Ceram. Int.*, 2021, **47**, 5374–5387, DOI: **10.1016/j.ceramint.2020.10.118**.

111 F. Ahmed and D. F. Rodrigues, Investigation of acute effects of graphene oxide on wastewater microbial community: A case study, *J. Hazard. Mater.*, 2013, **256–257**, 33–39, DOI: **10.1016/j.jhazmat.2013.03.064**.

112 M. Malakootian, A. Nasiri, A. Asadipour and E. Kargar, Facile and green synthesis of $ZnFe_2O_4$@ CMC as a new magnetic nanophotocatalyst for ciprofloxacin degradation from aqueous media, *Process Saf. Environ. Prot.*, 2019, **129**, 138–151.

113 M. Xie, W. Chen, Z. Xu, S. Zheng and D. Zhu, Adsorption of sulfonamides to demineralized pine wood biochars prepared under different thermochemical conditions, *Environ. Pollut.*, 2014, **186**, 187–194.

114 F. Tamaddon, M. H. Mosslemin, A. Asadipour, M. A. Gharaghani and A. Nasiri, Microwave-assisted preparation of $ZnFe_2O_4$@methyl cellulose as a new nano-biomagnetic photocatalyst for photodegradation of metronidazole, *Int. J. Biol. Macromol.*, 2020, **154**, 1036–1049, DOI: **10.1016/j.ijbiomac.2020.03.069**.

115 F. Tamaddon, A. Nasiri and G. Yazdanpanah, Photocatalytic degradation of ciprofloxacin using $CuFe_2O_4$@methyl cellulose based magnetic nanobiocomposite, *MethodsX*, 2020, **7**, 100764, DOI: **10.1016/j.mex.2019.12.005**.

116 S. Sutar, S. Otari and J. Jadhav, Biochar based photocatalyst for degradation of organic aqueous waste: A review, *Chemosphere*, 2022, **287**, 132200, DOI: **10.1016/j.chemosphere.2021.132200**.

117 M. M. Mian and G. Liu, Recent progress in biochar-supported photocatalysts: synthesis, role of biochar, and applications, *RSC Adv.*, 2018, **8**, 14237–14248.

118 S. Li, Z. Wang, X. Zhao, X. Yang, G. Liang and X. Xie, Insight into enhanced carbamazepine photodegradation over biochar-based magnetic photocatalyst Fe_3O_4/BiOBr/BC under visible LED light irradiation, *Chem. Eng. J.*, 2019, **360**, 600–611, DOI: **10.1016/j.cej.2018.12.002**.

119 M. Chen, Y. Dai, J. Guo, H. Yang, D. Liu and Y. Zhai, Solvothermal synthesis of biochar@$ZnFe_2O_4$/BiOBr Z-scheme heterojunction for efficient photocatalytic ciprofloxacin degradation under visible light, *Appl. Surf. Sci.*, 2019, **493**, 1361–1367, DOI: **10.1016/j.apsusc.2019.04.160**.

120 Z. Wang, X. Cai, X. Xie, S. Li, X. Zhang and Z. Wang, Visible-LED-light-driven photocatalytic degradation of ofloxacin and ciprofloxacin by magnetic biochar modified flower-like Bi_2WO_6: The synergistic effects, mechanism insights and degradation pathways, *Sci. Total Environ.*, 2021, **764**, 142879, DOI: **10.1016/j.scitotenv.2020.142879**.

121 Z. Wan, Y. Sun, D. C. Tsang, K. M. Iris, J. Fan, J. H. Clark, Y. Zhou, X. Cao, B. Gao and Y. S. Ok, A sustainable biochar catalyst synergized with copper heteroatoms and CO_2 for singlet oxygenation and electron transfer routes, *Green Chem.*, 2019, **21**, 4800–4814.

122 V. Doan, B. Huynh, H. A. L. Pham, Y. Vasseghian and V. T. Le, Cu_2O/Fe_3O_4/MIL-101Fe nanocomposite as a highly efficient and recyclable visible-light-driven catalyst for degradation of ciprofloxacin, *Environ. Res.*, 2021, **201**, 111593, DOI: **10.1016/j.envres.2021.111593**.

123 L. He, Y. Dong, Y. Zheng, Q. Jia, S. Shan and Y. Zhang, A novel magnetic MIL-101Fe/TiO_2 composite for photo degradation of tetracycline under solar light, *J. Hazard. Mater.*, 2019, **361**, 85–94, DOI: **10.1016/j.jhazmat.2018.08.079**.

124 X. Yang, J. Pan, J. Hu, S. Zhao and K. Cheng, MOF-derived La–$ZnFe_2O_4$@Fe_3O_4@carbon magnetic hybrid composite as a highly efficient and recyclable photocatalyst for mycotoxins degradation, *Chem. Eng. J.*, 2023, **467**, 143381.

125 X. Huang, Y. Chen, E. Walter, M. Zong, Y. Wang, X. Zhang, O. Qafoku, Z. Wang and K. M. Rosso, Facet-specific photocatalytic degradation of organics by heterogeneous fenton chemistry on hematite nanoparticles, *Environ. Sci. Technol.*, 2019, **53**, 10197–10207.

126 G. U. Rehman, M. Tahir, P. S. Goh, A. F. Ismail and I. U. Khan, Controlled synthesis of reduced graphene oxide supported magnetically separable Fe_3O_4@rGO@AgI ternary nanocomposite for enhanced photocatalytic degradation of phenol, *Powder Technol.*, 2019, **356**, 547–558, DOI: **10.1016/j.powtec.2019.08.026**.

127 S. Li, J. Cui, X. Wu, X. Zhang, Q. Hu and X. Hou, Rapid in situ microwave synthesis of Fe_3O_4@MIL-100Fe for aqueous diclofenac sodium removal through integrated adsorption and photodegradation, *J. Hazard. Mater.*, 2019, **373**, 408–416, DOI: **10.1016/j.jhazmat.2019.03.102**.

128 L. Yu, J. Chen, Z. Liang, W. Xu, L. Chen and D. Ye, Degradation of phenol using Fe_3O_4-GO nanocomposite as a heterogeneous photo-Fenton catalyst, *Sep. Purif. Technol.*, 2016, **171**, 80–87, DOI: **10.1016/j.seppur.2016.07.020**.

129 Q. Li, H. Kong, P. Li, J. Shao and Y. He, Photo-Fenton degradation of amoxicillin via magnetic TiO_2-graphene oxide-Fe_3O_4 composite with a submerged magnetic separation membrane photocatalytic reactor SMSMPR, *J. Hazard. Mater.*, 2019, **373**, 437–446, DOI: **10.1016/j.jhazmat.2019.03.066**.

130 Y. Xiang, Y. Huang, B. Xiao, X. Wu and G. Zhang, Magnetic yolk-shell structure of $ZnFe_2O_4$ nanoparticles for enhanced visible light photo-Fenton degradation towards antibiotics and mechanism study, *Appl. Surf. Sci.*, 2020, **513**, 145820, DOI: **10.1016/j.apsusc.2020.145820**.

131 L. Yang, Y. Xiang, F. Jia, L. Xia, C. Gao, X. Wu, L. Peng, J. Liu and S. Song, Photo-thermal synergy for boosting photo-Fenton activity with rGO-$ZnFe_2O_4$: Novel photo-activation process and mechanism toward environment remediation, *Appl. Catal., A*, 2021, **292**, 120198, DOI: **10.1016/j.apcatb.2021.120198**.

132 C. Lai, F. Huang, G. Zeng, D. Huang, L. Qin, M. Cheng, C. Zhang, B. Li, H. Yi, S. Liu, L. Li and L. Chen, Fabrication of novel magnetic $MnFe_2O_4$/bio-char composite and heterogeneous photo-Fenton degradation of tetracycline in near neutral pH, *Chemosphere*, 2019, **224**, 910–921, DOI: **10.1016/j.chemosphere.2019.02.193**.

133 W. Zhao, Z. Wei, X. Zhang, M. Ding, S. Huang and S. Yang, Magnetic recyclable $MnFe_2O_4$/CeO_2/SnS_2 ternary nano-photocatalyst for photo-Fenton degradation, *Appl. Catal., A*, 2020, **593**, 117443, DOI: **10.1016/j.apcata.2020.117443**.

134 B. Palanivel, C. Hu, M. Shkir, S. AlFaify, F. A. Ibrahim, M. S. Hamdy and A. Mani, Fluorine doped g-C_3N_4 coupled $NiFe_2O_4$ heterojunction: Consumption of H_2O_2 for production of hydroxyl radicals towards paracetamol degradation, *Colloid Interface Sci. Commun.*, 2021, **42**, 100410, DOI: **10.1016/j.colcom.2021.100410**.

135 M. Nawaz, A. Shahzad, K. Tahir, J. Kim, M. Moztahida, J. Jang, M. B. Alam, S. Lee, H. Jung and D. S. Lee, Photo-Fenton reaction for the degradation of sulfamethoxazole using a multi-walled carbon nanotube-$NiFe_2O_4$ composite, *Chem. Eng. J.*, 2020, **382**, 123053.

136 K. A. Azalok, A. A. Oladipo and M. Gazi, Hybrid MnFe-LDO–biochar nanopowders for degradation of metronidazole via UV-light-driven photocatalysis: Characterization and mechanism studies, *Chemosphere*, 2021, **268**, 128844, DOI: **10.1016/j.chemosphere.2020.128844**.

137 S. Dudziak, Z. Bielan, P. Kubica and A. Zielińska-Jurek, Optimization of carbamazepine photodegradation on defective TiO_2-based magnetic photocatalyst, *J. Environ. Chem. Eng.*, 2021, **9**, 105782, DOI: **10.1016/j.jece.2021.105782**.

138 X. Wang, H. Jin, D. Wu, Y. Nie, X. Tian, C. Yang, Z. Zhou and Y. Li, Fe_3O_4@S-doped ZnO: A magnetic, recoverable, and reusable Fenton-like catalyst for efficient degradation of ofloxacin under alkaline conditions, *Environ. Res.*, 2020, **186**, 109626, DOI: **10.1016/j.envres.2020.109626**.

139 F. Wang, Y. Chen, R. Zhu and J. Sun, Novel synthesis of magnetic, porous C/$ZnFe_2O_4$ photocatalyst with enhanced activity under visible light based on the Fenton-like reaction, *Dalton Trans.*, 2017, **46**, 11306–11317.

140 W. An, S. Hu, C. Liu, J. Hu, H. Wang, W. Cui and Y. Liang, 2D sheet structure $Bi_{24}O_{31}C_{l10}$ hybridized with Fe_2O_3 nanoparticles for improved photocatalytic-Fenton synergistic degradation performance, *Mater. Chem. Phys.*, 2023, **295**, 127152, DOI: **10.1016/j.matchemphys.2022.127152**.

141 W. S. Hamd and J. Dutta, in *Nanomaterials for the Detection and Removal of Wastewater Pollutants*, Elsevier, 2020, pp. 303–330.

142 D. Hermosilla, C. Han, M. N. Nadagouda, L. Machala, A. Gascó, P. Campo and D. D. Dionysiou, Environmentally friendly synthesized and magnetically recoverable designed ferrite photo-catalysts for wastewater treatment applications, *J. Hazard. Mater.*, 2020, **381**, 121200, DOI: **10.1016/j.jhazmat.2019.121200**.

143 W. F. Elmobarak, B. H. Hameed, F. Almomani and A. Z. Abdullah, A review on the treatment of petroleum refinery wastewater using advanced oxidation processes, *Catalysts*, 2021, **11**, 782.

144 A. Asghar, A. A. A. Raman and W. M. A. W. Daud, Advanced oxidation processes for in-situ production of hydrogen peroxide/hydroxyl radical for textile wastewater treatment: a review, *J. Cleaner Prod.*, 2015, **87**, 826–838.

145 Y. Liu, Y. Zhao and J. Wang, Fenton/Fenton-like processes with in-situ production of hydrogen peroxide/hydroxyl radical for degradation of emerging contaminants: Advances and prospects, *J. Hazard. Mater.*, 2021, **404**, 124191, DOI: **10.1016/j.jhazmat.2020.124191**.

146 S. O. Ganiyu, M. Zhou and C. A. Martínez-Huitle, Heterogeneous electro-Fenton and photoelectro-Fenton processes: A critical review of fundamental principles and application for water/wastewater treatment, *Appl. Catal., B*, 2018, **235**, 103–129, DOI: **10.1016/j.apcatb.2018.04.044**.

147 X. Wang, X. Zhang, Y. Zhang, Y. Wang, S. Sun, W. D. Wu and Z. Wu, Nanostructured semiconductor supported iron catalysts for heterogeneous photo-Fenton oxidation: a review, *J. Mater. Chem. A*, 2020, **8**, 15513–15546.

148 R. Matta, S. Tlili, S. Chiron and S. Barbati, Removal of carbamazepine from urban wastewater by sulfate radical oxidation, *Environ. Chem. Lett.*, 2011, **9**, 347–353.

149 K. A. Lin and Z. Zhang, Degradation of Bisphenol A using peroxymonosulfate activated by one-step prepared sulfur-doped carbon nitride as a metal-free heterogeneous catalyst, *Chem. Eng. J.*, 2017, **313**, 1320–1327.

150 W. Wang, M. Chen, D. Wang, M. Yan and Z. Liu, Different activation methods in sulfate radical-based oxidation for organic pollutants degradation: Catalytic mechanism and toxicity assessment of degradation intermediates, *Sci. Total Environ.*, 2021, **772**, 145522.

151 S. Giannakis, K. A. Lin and F. Ghanbari, A review of the recent advances on the treatment of industrial wastewaters by Sulfate Radical-based Advanced Oxidation Processes SR-AOPs, *Chem. Eng. J.*, 2021, **406**, 127083, DOI: **10.1016/j.cej.2020.127083**.

152 Y. Zhong, K. Shih, Z. Diao, G. Song, M. Su, L. Hou, D. Chen and L. Kong, Peroxymonosulfate activation through LED-induced $ZnFe_2O_4$ for levofloxacin degradation, *Chem. Eng. J.*, 2021, **417**, 129225, DOI: **10.1016/j.cej.2021.129225**.

153 M. Kohantorabi, G. Moussavi, P. Oulego and S. Giannakis, Radical-based degradation of sulfamethoxazole via UVA/PMS-assisted photocatalysis, driven by magnetically separable Fe_3O_4@CeO_2@BiOI nanospheres, *Sep. Purif. Technol.*, 2021, **267**, 118665, DOI: **10.1016/j.seppur.2021.118665**.

154 M. Noorisepehr, K. Ghadirinejad, B. Kakavandi, A. Ramazanpour Esfahani and A. Asadi, Photo-assisted catalytic degradation of acetaminophen using peroxymonosulfate decomposed by magnetic carbon heterojunction catalyst, *Chemosphere*, 2019, **232**, 140–151, DOI: **10.1016/j.chemosphere.2019.05.070**.

155 S. S. Rezaei, B. Kakavandi, M. Noorisepehr, A. A. Isari, S. Zabih and P. Bashardoust, Photocatalytic oxidation of tetracycline by magnetic carbon-supported TiO_2 nanoparticles catalyzed peroxydisulfate: Performance, synergy and reaction mechanism studies, *Sep. Purif. Technol.*, 2021, **258**, 117936, DOI: **10.1016/j.seppur.2020.117936**.

156 Y. Wu, Z. Fang, Y. Shi, H. Chen, Y. Liu, Y. Wang and W. Dong, Activation of peroxymonosulfate by BiOCl@Fe_3O_4 catalyst for the degradation of atenolol: Kinetics, parameters, products and mechanism, *Chemosphere*, 2019, **216**, 248–257, DOI: **10.1016/j.chemosphere.2018.10.012**.

157 Z. Zheng, J. Min, X. Wang, C. W. Lung, K. Shih and I. M. C. Lo, Directional separation of highly reductive electrons to the reactive center in a magnetic S-scheme $ZnFe_2O_4$/A-MoS_2 heterojunction for enhanced peroxymonosulfate activation

toward pharmaceuticals and personal care product removal, *Environ. Sci. Technol.*, 2023, **57**, 8414–8425, DOI: **10.1021/acs.est.2c09122**.

158 M. Jia, Z. Yang, W. Xiong, J. Cao, Y. Xiang, H. Peng, Y. Jing, C. Zhang, H. Xu and P. Song, Magnetic heterojunction of oxygen-deficient Ti^{3+}-TiO_2 and Ar-Fe_2O_3 derived from metal-organic frameworks for efficient peroxydisulfate PDS photo-activation, *Appl. Catal., B*, 2021, **298**, 120513, DOI: **10.1016/j.apcatb.2021.120513**.

159 A. A. Isari, S. Moradi, S. S. Rezaei, F. Ghanbari, E. Dehghanifard and B. Kakavandi, Peroxymonosulfate catalyzed by core/shell magnetic ZnO photocatalyst towards malathion degradation: Enhancing synergy, catalytic performance and mechanism, *Sep. Purif. Technol.*, 2021, **275**, 119163, DOI: **10.1016/j.seppur.2021.119163**.

160 Q. Yang, Y. Ma, F. Chen, F. Yao, J. Sun, S. Wang, K. Yi, L. Hou, X. Li and D. Wang, Recent advances in photo-activated sulfate radical-advanced oxidation process SR-AOP for refractory organic pollutants removal in water, *Chem. Eng. J.*, 2019, **378**, 122149, DOI: **10.1016/j.cej.2019.122149**.

161 S. Feng, T. Xie, J. Wang, J. Yang, D. Kong, C. Liu, S. Chen, F. Yang, M. Pan, J. Yang, H. Du and H. Chen, Photocatalytic activation of PMS over magnetic heterojunction photocatalyst $SrTiO_3$/$BaFe_{12}O_{19}$ for tetracycline ultrafast degradation, *Chem. Eng. J.*, 2023, **470**, 143900.

162 X. Yan, T. Zhang, S. Meng, P. Zhou, Y. Xu, Y. Wang and M. Xie, $BaFe_{12}O_{19}$/BiOBr S-scheme heterojunction magnetic nanosheets for high-efficiency photocatalytic degradation of 2-mercaptobenzothiazole, *Sep. Purif. Technol.*, 2023, **326**, 124746.

163 W. Oh, S. Lua, Z. Dong and T. Lim, High surface area DPA-hematite for efficient detoxification of bisphenol A via peroxymonosulfate activation, *J. Mater. Chem. A*, 2014, **2**, 15836–15845.

164 C. Dong, Z. Wang, Z. Ye, J. He, Z. Zheng, X. Gong, J. Zhang and I. M. C. Lo, Superoxide radicals dominated visible light driven peroxymonosulfate activation using molybdenum selenide $MoSe_2$ for boosting catalytic degradation of pharmaceuticals and personal care products, *Appl. Catal., B*, 2021, **296**, 120223, DOI: **10.1016/j.apcatb.2021.120223**.

165 L. Li, X. Yuan, Z. Zhou, R. Tang, Y. Deng, Y. Huang, S. Xiong, L. Su, J. Zhao and D. Gong, Research progress of photocatalytic activated persulfate removal of environmental organic pollutants by metal and nonmetal based photocatalysts, *J. Cleaner Prod.*, 2022, **372**, 133420, DOI: **10.1016/j.jclepro.2022.133420**.

166 A. Mahmoud and R. S. Freire, Métodos emergentes para aumentar a eficiência do ozônio no tratamento de águas contaminadas, *Quim. Nova*, 2007, **30**, 198–205.

167 M. Ye, Z. Chen, X. Liu, Y. Ben and J. Shen, Ozone enhanced activity of aqueous titanium dioxide suspensions for photodegradation of 4-chloronitrobenzene, *J. Hazard. Mater.*, 2009, **167**, 1021–1027, DOI: **10.1016/j.jhazmat.2009.01.091**.

168 N. M. Mahmoodi, M. Bashiri and S. J. Moeen, Synthesis of nickel–zinc ferrite magnetic nanoparticle and dye degradation using photocatalytic ozonation, *Mater. Res. Bull.*, 2012, **47**, 4403–4408, DOI: **10.1016/j.materresbull.2012.09.036**.

169 D. H. Quiñones, A. Rey, P. M. Álvarez, F. J. Beltrán and P. K. Plucinski, Enhanced activity and reusability of TiO_2 loaded magnetic activated carbon for solar photocatalytic ozonation, *Appl. Catal., B*, 2014, **144**, 96–106, DOI: **10.1016/j.apcatb.2013.07.005**.

170 Y. Ling, H. Liu, B. Li, B. Zhang, Y. Wu, H. Hu, D. Yu and S. Huang, Efficient photocatalytic ozonation of azithromycin by three-dimensional g-C_3N_4 nanosheet loaded magnetic Fe-MCM-48 under simulated solar light, *Appl. Catal., B*, 2023, **324**, 122208, DOI: **10.1016/j.apcatb.2022.122208**.

171 Y. Gao, B. Yang, Y. Yang, H. Ming, G. Liu, J. Zhang and Y. Hou, Carbon-coated $ZnFe_2O_4$ nanoparticles as an efficient, robust and recyclable catalyst for photocatalytic ozonation of organic pollutants, *J. Environ. Chem. Eng.*, 2022, **10**, 107419, DOI: **10.1016/j.jece.2022.107419**.

172 J. Yin, G. Liao, J. Zhou, C. Huang, Y. Ling, P. Lu and L. Li, High performance of magnetic $BiFeO_3$ nanoparticle-mediated photocatalytic ozonation for wastewater decontamination, *Sep. Purif. Technol.*, 2016, **168**, 134–140, DOI: **10.1016/j.seppur.2016.05.049**.

173 A. M. Chávez, D. H. Quiñones, A. Rey, F. J. Beltrán and P. M. Álvarez, Simulated solar photocatalytic ozonation of contaminants of emerging concern and effluent organic matter in secondary effluents by a reusable magnetic catalyst, *Chem. Eng. J.*, 2020, **398**, 125642, DOI: **10.1016/j.cej.2020.125642**.

174 L. Ciccotti, L. do Vale, T. L. R. Hewer and R. S. Freire, Fe_3O_4@TiO_2 preparation and catalytic activity in heterogeneous photocatalytic and ozonation processes, *Catal. Sci. Technol.*, 2015, **5**, 1143–1152.

175 M. Aram, M. Farhadian, A. R. Solaimany Nazar, S. Tangestaninejad, P. Eskandari and B. Jeon, Metronidazole and Cephalexin degradation by using of Urea/TiO_2/$ZnFe_2O_4$/Clinoptiloite catalyst under visible-light irradiation and ozone injection, *J. Mol. Liq.*, 2020, **304**, 112764, DOI: **10.1016/j.molliq.2020.112764**.

176 A. Kumar, A. Kumar, G. Sharma, M. Naushad, F. J. Stadler, A. A. Ghfar, P. Dhiman and R. V. Saini, Sustainable nano-hybrids of magnetic biochar supported g-C_3N_4/$FeVO_4$ for solar powered degradation of noxious pollutants- Synergism of adsorption, photocatalysis & photo-ozonation, *J. Cleaner Prod.*, 2017, **165**, 431–451, DOI: **10.1016/j.jclepro.2017.07.117**.

177 J. Xiao, Y. Xie and H. Cao, Organic pollutants removal in wastewater by heterogeneous photocatalytic ozonation, *Chemosphere*, 2015, **121**, 1–17.

178 B. Lashuk and V. Yargeau, A review of ecotoxicity reduction in contaminated waters by heterogeneous photocatalytic ozonation, *Sci. Total Environ.*, 2021, **787**, 147645, DOI: **10.1016/j.scitotenv.2021.147645**.

179 M. M. Sein, M. Zedda, J. Tuerk, T. C. Schmidt, A. Golloch and C. Von Sonntag, Oxidation of diclofenac with ozone in aqueous solution, *Environ. Sci. Technol.*, 2008, **42**, 6656–6662.

180 M. Mehrjouei, S. Müller and D. Möller, A review on photocatalytic ozonation used for the treatment of water and wastewater, *Chem. Eng. J.*, 2015, **263**, 209–219, DOI: **10.1016/j.cej.2014.10.112**.

181 N. F. F. Moreira, C. A. Orge, A. R. Ribeiro, J. L. Faria, O. C. Nunes, M. F. R. Pereira and A. M. T. Silva, Fast mineralization and detoxification of amoxicillin and diclofenac by photocatalytic ozonation and application to an urban wastewater, *Water Res.*, 2015, **87**, 87–96, DOI: **10.1016/j.watres.2015.08.059**.

182 M. H. Abdurahman, A. Z. Abdullah and N. F. Shoparwe, A comprehensive review on sonocatalytic, photocatalytic, and sonophotocatalytic processes for the degradation of antibiotics in water: Synergistic mechanism and degradation pathway, *Chem. Eng. J.*, 2021, **413**, 127412, DOI: **10.1016/j.cej.2020.127412**.

183 V. F. Humphrey, Ultrasound and matter—Physical interactions, *Prog. Biophys. Mol. Biol.*, 2007, **93**, 195–211, DOI: **10.1016/j.pbiomolbio.2006.07.024**.

184 J. He, C. Dong, X. Chen, H. Cai, X. Chen, X. Jiang, Y. Zhang, A. Peng and M. A. Badsha, Review of piezocatalysis and piezo-assisted photocatalysis in environmental engineering, *Crystals*, 2023, **13**, 1382.

185 D. K. Gorai, S. K. Kuila, A. Oraon, A. Kumar, M. Suthar, R. Mitra, K. Biswas, P. K. Roy, M. I. Ahmad and T. K. Kundu, A facile and green synthesis of Mn and P functionalized graphitic carbon nitride nanosheets for spintronics devices and enhanced photocatalytic performance under visible-light, *J. Colloid Interface Sci.*, 2023, **644**, 397–414.

186 A. Zhou, L. Liao, X. Wu, K. Yang, C. Li, W. Chen and P. Xie, Fabrication of a Z-scheme nanocomposite photocatalyst for enhanced photocatalytic degradation of ibuprofen under visible light irradiation, *Sep. Purif. Technol.*, 2020, **250**, 117241, DOI: **10.1016/j.seppur.2020.117241**.

187 S. Ahmed, Y. Zhang, B. Wu, Z. Zheng, C. F. Leung, T. Y. Choy, Y. T. Kwok and I. M. Lo, Scaled-up development of magnetically recyclable Fe_3O_4/$LaOH_3$ composite for river water phosphate removal: From bench-scale to pilot-scale study, *Sci. Total Environ.*, 2021, **791**, 148281, DOI: **10.1016/j.scitotenv.2021.148281**.

188 G. Zhao, J. Ding, F. Zhou, X. Chen, L. Wei, Q. Gao, K. Wang and Q. Zhao, Construction of a visible-light-driven magnetic dual Z-scheme $BiVO_4$/g-C_3N_4/$NiFe_2O_4$ photocatalyst for effective removal of ofloxacin: Mechanisms and degradation pathway, *Chem. Eng. J.*, 2021, **405**, 126704, DOI: **10.1016/j.cej.2020.126704**.

189 L. Li, C. Niu, H. Guo, J. Wang, M. Ruan, L. Zhang, C. Liang, H. Liu and Y. Yang, Efficient degradation of Levofloxacin with magnetically separable $ZnFe_2O_4$/NCDs/Ag_2CO_3 Z-scheme heterojunction photocatalyst: Vis-NIR light response ability and mechanism insight, *Chem. Eng. J.*, 2020, **383**, 123192, DOI: **10.1016/j.cej.2019.123192**.

190 C. Guo, S. Gao, J. Lv, S. Hou, Y. Zhang and J. Xu, Assessing the photocatalytic transformation of norfloxacin by BiOBr/iron oxides hybrid photocatalyst: Kinetics, intermediates, and influencing factors, *Appl. Catal., B*, 2017, **205**, 68–77, DOI: **10.1016/j.apcatb.2016.12.032**.

191 J. Iannicelli, New developments in magnetic separation, *IEEE Trans. Magn.*, 1976, **12**, 436–443.

